Bioactive Materials 37 (2024) 331–347

Contents lists available at ScienceDirect

Bioactive Materials

journal homepage: www.keaipublishing.com/en/journals/bioactive-materials

Injectable thermo-sensitive hydrogel enhances anti-tumor potency of engineered *Lactococcus lactis* by activating dendritic cells and effective memory T cells

Aoxing Chen [a], Junmeng Zhu [b], Rui Liu [c], Yi Mei [b], Lin Li [b], Yue Fan [c], Yaohua Ke [b], Baorui Liu [a,b,**], Qin Liu [a,b,*]

[a] Department of Oncology, Nanjing Drum Tower Hospital Clinical College of Nanjing University of Chinese Medicine, The Clinical Cancer Institute of Nanjing University, 321 Zhongshan Road, Nanjing, 210008, China
[b] The Comprehensive Cancer Centre, Nanjing Drum Tower Hospital, Affiliated Hospital of Medical School, Nanjing University, 321 Zhongshan Road, Nanjing, 210008, China
[c] The Comprehensive Cancer Centre, China Pharmaceutical University Nanjing Drum Tower Hospital, 321 Zhongshan Road, Nanjing, 210008, China

ARTICLE INFO

Keywords:
Cancer immunotherapy
Engineered bacteria
Thermos-sensitive hydrogel
Localized drug delivery
Artificial lymph node

ABSTRACT

Engineered bacteria have shown great potential in cancer immunotherapy by dynamically releasing therapeutic payloads and inducing sustained antitumor immune response with the crosstalk of immune cells. In previous studies, FOLactis was designed, which could secret an encoded fusion protein of Fms-related tyrosine kinase 3 ligand and co-stimulator OX40 ligand, leading to remarkable tumor suppression and exerting an abscopal effect by intratumoral injection. However, it is difficult for intratumoral administration of FOLactis in solid tumors with firm texture or high internal pressure. For patients without lesions such as abdominal metastatic tumors and orthotopic gastric tumors, intratumoral injection is not feasible and peritumoral maybe a better choice. Herein, an engineered bacteria delivery system is constructed based on in situ temperature-sensitive poloxamer 407 hydrogels. Peritumoral injection of FOLactis/P407 results in a 5-fold increase in the proportion of activated DC cells and a more than 2-fold increase in the proportion of effective memory T cells (T_{EM}), playing the role of artificial lymph island. Besides, administration of FOLactis/P407 significantly inhibits the growth of abdominal metastatic tumors and orthotopic gastric tumors, resulting in an extended survival time. Therefore, these findings demonstrate the delivery approach of engineered bacteria based on in situ hydrogel will promote the efficacy and universality of therapeutics.

1. Introduction

Immunotherapy has been widely confirmed as one of the most critical approaches to attack tumors [1–3]. Immune infiltration, particularly by dendritic cells (DCs) and T lymphocytes, usually greatly influences the efficacy of immunotherapy [4,5]. Nevertheless, only few DCs, as well as T cells, exist in tumors typically, while part of them are inactive due to tumor-suppressor factors [6,7]. Small molecule drugs, such as cytokines and antibodies, were administered to lead to DCs recruitment and T cell activation [8]. For example, intratumoral injection of Fms-like tyrosine kinase 3 ligand (Flt3L) and OX40 agonists has been demonstrated in the preclinical research and clinical trial [9,10]. However, due to the rapid metabolism via the tumor vasculature and/or lymphatics, persistent concentration of small-molecule drugs is hard to maintain locally. Recently, intelligent delivery systems based on microorganisms and exosomes were designed and applied for remedy owing to the rapid development of synthetic biology [11,12]. Probiotics were found in the human gut, and the antitumor effect of lactis has been proved [13,14].

Based on the theories above, we designed a bifunctional engineered *Lactococcus lactis* (FOLactis), delivering an encoded fusion protein of

Peer review under responsibility of KeAi Communications Co., Ltd.

* Corresponding author. Department of Oncology, Nanjing Drum Tower Hospital Clinical College of Nanjing University of Chinese Medicine, The Clinical Cancer Institute of Nanjing University, 321 Zhongshan Road, Nanjing, 210008, China.
** Corresponding author. The Comprehensive Cancer Centre, Nanjing Drum Tower Hospital, Affiliated Hospital of Medical School, Nanjing University, 321 Zhongshan Road, Nanjing, 210008, China.
E-mail addresses: baoruiliu@nju.edu.cn (B. Liu), liuqin@nju.edu.cn (Q. Liu).

https://doi.org/10.1016/j.bioactmat.2024.03.023
Received 16 November 2023; Received in revised form 20 February 2024; Accepted 15 March 2024

Flt3L and co-stimulator OX40 ligand (OX40L) [15]. Intratumoral injection of FOLactis could eliminate tumor growth through cell lysis and induce mass tumor-specific antigens release [16,17]. In addition, Flt3L expressing FOLactis can expand conventional-type-1-dendritic cells (cDC1), while FOLactis expressing OX40L promotes tumor infiltrating effector T cells (Teff) activation [18]. Thus, FOLactis leads to remarkable tumor suppression and exerts an abscopal effect due to its in situ vaccination (ISV) effect. However, the approach of FOLactis administration needs to be optimized ulteriorly due to the complexity and diversity of tumors. Reports from preclinical and clinical studies also show some obstacles, such as bacterial viability, local and systemic infection risk, and first-pass effect that restrict the clinical translation of surface-modified bacteria [19,20]. Firstly, part of tumor-bearing mice recurred 3–4 weeks after treatment, especially in 'cold' models, meaning the ISV effect of FOLactis is still not persistent [15]. On top of this, intratumoral administration of FOLactis is difficult to perform for patients with advanced metastatic tumors like gastrointestinal tumors and ovarian tumors. In addition, it is hard for pure FOLactis to retent at/near the tumor side for a long time due to rapid metabolism after injection, especially in metastatic models. Furthermore, repeated intratumoral injections necessitate patient compliance. Therefore, it is imperative to develop an efficient carrier to take full advantage of FOLactis.

Over the past few decades, drug delivery systems like hydrogels, nanoparticles, and microspheres have been designed for cancer immunotherapy to prolong the reside time of anticancer drugs [21–24]. Among them, injectable hydrogel has become a promising approach for sustained and local delivery of engineered bacteria [25]. Biodegradable thermo-sensitive hydrogels, which have the characteristic of temperature-responsive 'sol-gel' transition, are excellent options for sustained release and local drug delivery [26]. At room temperature, thermo-sensitive hydrogels allow loading drugs readily and integrally. Once exposed to physiological temperature, the drug-loading formulations undergo a 'sol-gel' transition, then turn into hydrogel spontaneously and contribute to drug release in the site. The outstanding adherence and mechanical strength of hydrogel allow sustained drug release and long-term anti-tumor efficacy through single administration. Poloxamer 407 (P407, F127) is a biocompatible FDA-approved polymer made up of poly (ethylene oxide)-poly (propylene oxide)-poly (ethylene

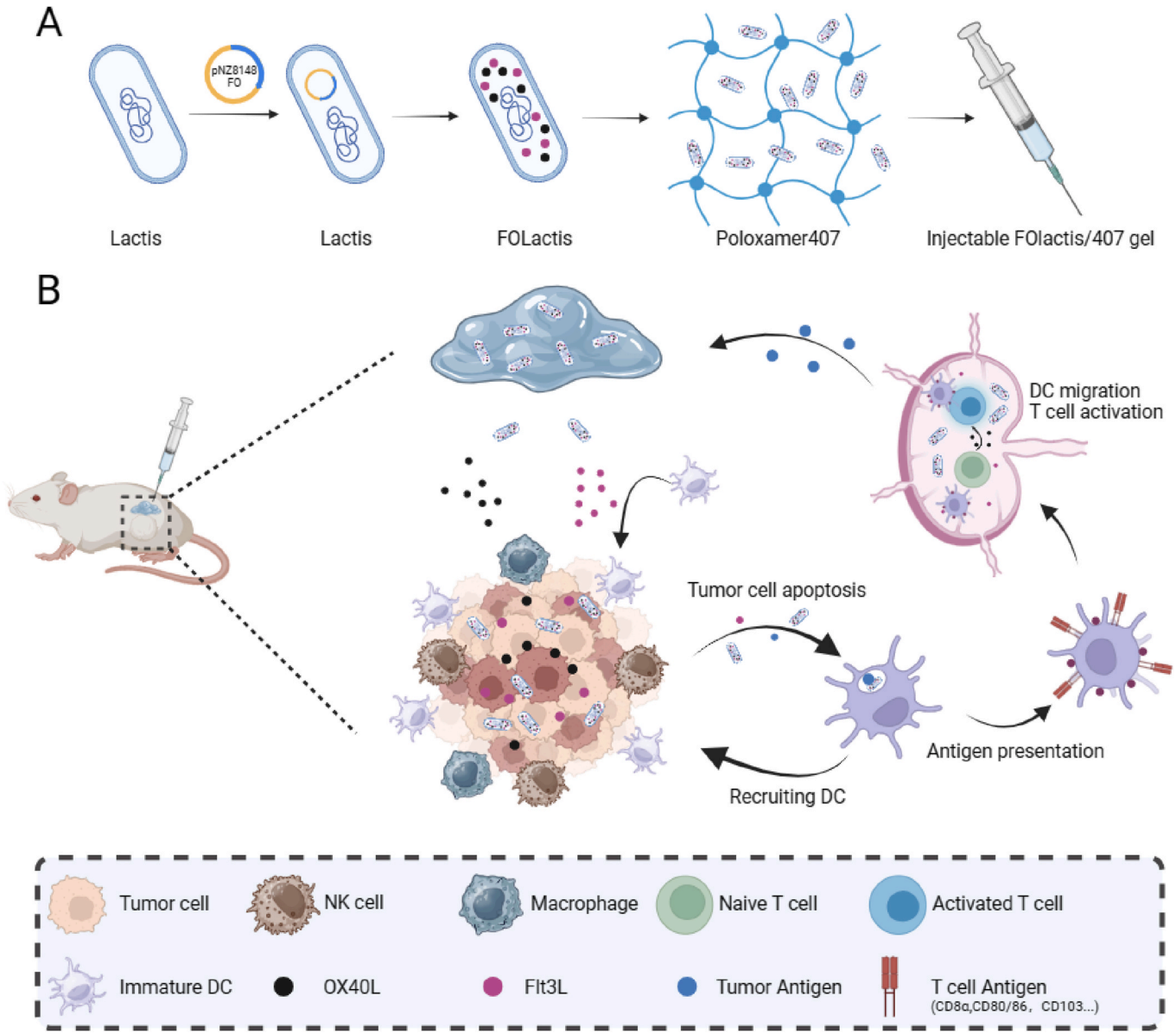

Scheme 1. Schematic diagram of in situ sustained delivery system of engineered Lactococcus lactis (FOLactis) via injectable thermo-sensitive poloxamer P407 hydrogel. A) Preparation of injectable in situ FOLactis/P407 hydrogel. B) The immune response induced by in situ FOLactis/P407 hydrogel in vivo.

oxide) triblock copolymers (EO-PO-EO) [27]. When dissolved in cold solution, the polymers assembled micelles consisting of hydrophobic PO core and hydrophilic EO outer shell. The micelles formatted rigid network and then gelated for P407 under enough concentrations once the temperature reached the critical gelation temperature (CGT) [28]. The P407 then serves as a depot to slow release, limiting the systemic distribution of the drug. Injectable in situ hydrogels based on poloxamer have drawn significant attention in anti-tumor drug delivery [29,30]. Studies have shown in situ P407 hydrogel treatment inhibits tumor growth significantly while reducing systemic drug concentration and side effects [31].

In this study, we design a bacteria delivery system for cancer immunotherapy based on biodegradable temperature-sensitive poloxamer 407 hydrogels. FOLactis primarily kills cancer cells through cell lysis, leading to the release of tumor-specific antigens into hydrogel. Flt3L expressing FOLactis released from in situ P407 hydrogel prompts recruitment and activation of immature DCs. Then, OX40L released from FOLactis/P407 enhances the expression of OX40 on $CD4^+$ T cells in TME by PAMPs and promotes tumor infiltrating effector T cells (T_{eff}) activation. Moreover, encapsulated FOLactis can release sustainedly and serve as a long-acting depot, prolonging the local maintenance time of drugs and inhibiting tumor growth in the long term, functioning as an artificial lymph island at the tumor side. Our study shows that in situ FOLactis/P407 has a long-term anti-tumor effect by adhering and distributing to adjacent tissue and the abdominal cavity. Besides, the slow-release effect and biocompatibility of P407 hydrogel reduce the potential local and systemic toxicity of FOLactis (Scheme 1). Overall, our study indicates a strategy to encapsulate engineered bacteria into thermos-sensitive in situ hydrogel to enhance tumor immunotherapy for a long-time, which could play the role of lymph island with the potential for clinical translation.

2. Results

2.1. Preparation and characterization of FOLactis/P407

It has been widely reported that the time to gelation kinetics of poloxamer 407 hydrogel depends on concentration and temperature [27,32]. In order to combine P407 and FOLactis into an artificial lymph island better, we need to consider the parameters such as gel pore size and drug release rate. To meet our requirements, the time to gelation of P407 hydrogel under different concentrations at RT (20 °C) and body temperature (37 °C) was measured and customed for the follow-up experiment. The results showed that 16% P407 could not gelate at both RT and body temperature, while the gelation time of 25% P407 was 198s and reduced gradually. Meanwhile, concentration ≥25% may have disadvantages of prompt gelation at RT (129s and 98s for 30% and 35% concentration, respectively; Fig. 1A) and typically have sol-gel transition temperatures below 15 °C [27]. As concentration of P407 hydrogel rose, gelation time decreased significantly at physiological temperature (52s for 20%, 29s for 25%, 22s for 30%, and 19s for 35%; Fig. 1B). It should be noted that 20% P407 only has a sol-gel transition at body temperature, which could be an ideal concentration for the FOLactis hydrogel delivery system. Since the water content of the P407 hydrogel was above 80%, the composite system was almost a suspension of dissolved drugs and micelles at RT enabling sufficient time for us to inject drugs at 20 °C. The addition of FOLactis did not influence gelation time at both RT and body temperature (Fig. 1C and D).

As shown in Fig. 1E, the P407 hydrogel (20 wt%) had good fluidity at RT, and underwent sol-gel transition when the temperature increased to 37 °C, which was similar to the mixed FOLactis/P407 hydrogel (5×10^9 CFU FOLactis and 20 wt% P407). For subsequent applications, such as subcutaneous and intraperitoneal injection, we detected the in situ injectability and gelation of FOLactis/P407. The injection was performed readily through a 24G syringe needle at 20 °C without the risk of syringe needle clogging. Besides, we observed rapid gelation in situ and maintained stable FOLactis/P407 hydrogel when injected into in NS at 37 °C, which means its potential feasibility of gelation in subcutaneous tissue and peritoneal cavity (Fig. 1F).

P407 could self-assemble into micelles because of its amphipathic properties in water [33,34]. As we measured by DLS (Dynamic light scattering), P407 micelles already started to form from 2.5 to 7.5% concentration. A representative size distribution histogram of the micelles at 5% P407 was depicted in Fig. 1G. As shown in Fig. 1H and I, the average micelle was 30 nm with PDI of 0.37 at 2.5% concentration. For 5% concentration, the average micelle was 31 nm with a PDI of 0.36 at 5% concentration, which is similar to 7.5% concentration (Z-ave:29 nm and PDI:0.39). The micelles are small at room temperature. When exposed temperature increased to 37 °C, a micellar network can generate spontaneously since the boost in micelles size and the sharp aggregation between augmented micelles, finally leading to a physical hydrogel. Furthermore, we observed the mechanical properties and sol-gel translation of FOLactis/P407 hydrogels through dynamic rheological measurements. The detection occurred in the temperature range of 10–40 °C with the strain and angular frequency were fixed as 2% and 10 rad s^{-1}, respectively, the heating rate was 1 °C min^{-1}. As shown in Fig. 1J, blank P407 hydrogel (20 wt%) went through temperature-responsive gelation characteristic by showing low storage modules (G′) and loss modules (G″) at low temperature and increased signally as the temperature rose to about 27 °C with the appearance of crosspoint between G′ and G″, which means gelation of FOLactis/P407. As temperature increase continuedly, G′ and G″ became stable gradually until termination, the former is 8298Pa, which represents the mechanical strength of hydrogel, while the other is 1131Pa. The sol-gel translation and mechanical properties of P407 hydrogel hardly altered while loading FOLactis (Fig. 1K).

The scanning electron microscope (SEM) images indicated the abundant porous structure of the FOLactis/P407 hydrogel (20 wt%) with a pore size of 50–70 μm from 150 × magnifications, which is hardly varied compared to blank P407 hydrogel (Fig. 1L). The FOLactis displayed typical coccus with a diameter of 1–2 μm in the hydrogel from 3000 × magnifications (Fig. 1M), which has been reported previously [15,35]. Besides, both FOLactis and the aperture of P407 are micron-sized, and bacteria maybe trapped in hydrogel without delivery, thus, to ensure the smooth release of FOLactis from P407, FOLactis/P407 hydrogel (16 wt%) was also measured to detect the relationship between bore diameter and hydrogel concentration. The FOLactis/P407 hydrogel (16 wt%) exhibited abundant porous structure with a pore size of 70–90 nm from 150 × magnifications (Fig. 1N), which means lower concentration usually results in larger bore diameter, in line with previous reports [36]. Besides, blank P407 hydrogel at 16% and 30% were also measured to detect the correlation between sol-gel phase transition behavior and concentration. 16% concentration hydrogel shows higher gelation temperature and lower mechanical strength when gelation (Figs. S1A and B, Supporting Information), which is opposite to 30% concentration hydrogel. Moreover, FTIR and H-NMR analysis (Figs. S1C and D, Supporting Information) were comparable with data that is available in literature [37,38], proving the purity of P407 powder.

2.2. Release of FOLactis from the P407 hydrogel both in vivo and in vitro

Firstly, we investigated FOLactis release from the P407 hydrogel (20 wt%) in vitro. As shown in Fig. 2A, P407 hydrogel shows burst release relatively at initial time with nearly 50% releasement of the loaded amount of FOLactis within 24 h. After 5 days, over 95% loading amount of FOLactis was released from P407 hydrogel. Overall, FOLactis/P407 hydrogel released FOLactis sustainably for up to 5 days, mainly in line with the degradation of P407 hydrogel (Fig. 2B). Besides, we detected whether P407 hydrogel would restrict the release of FO fusion protein as FOLactis died. As shown in Fig. S2, P407 hydrogel slowed the release rate of FO fusion protein by about half on 30 days (16% in P407 and 30%

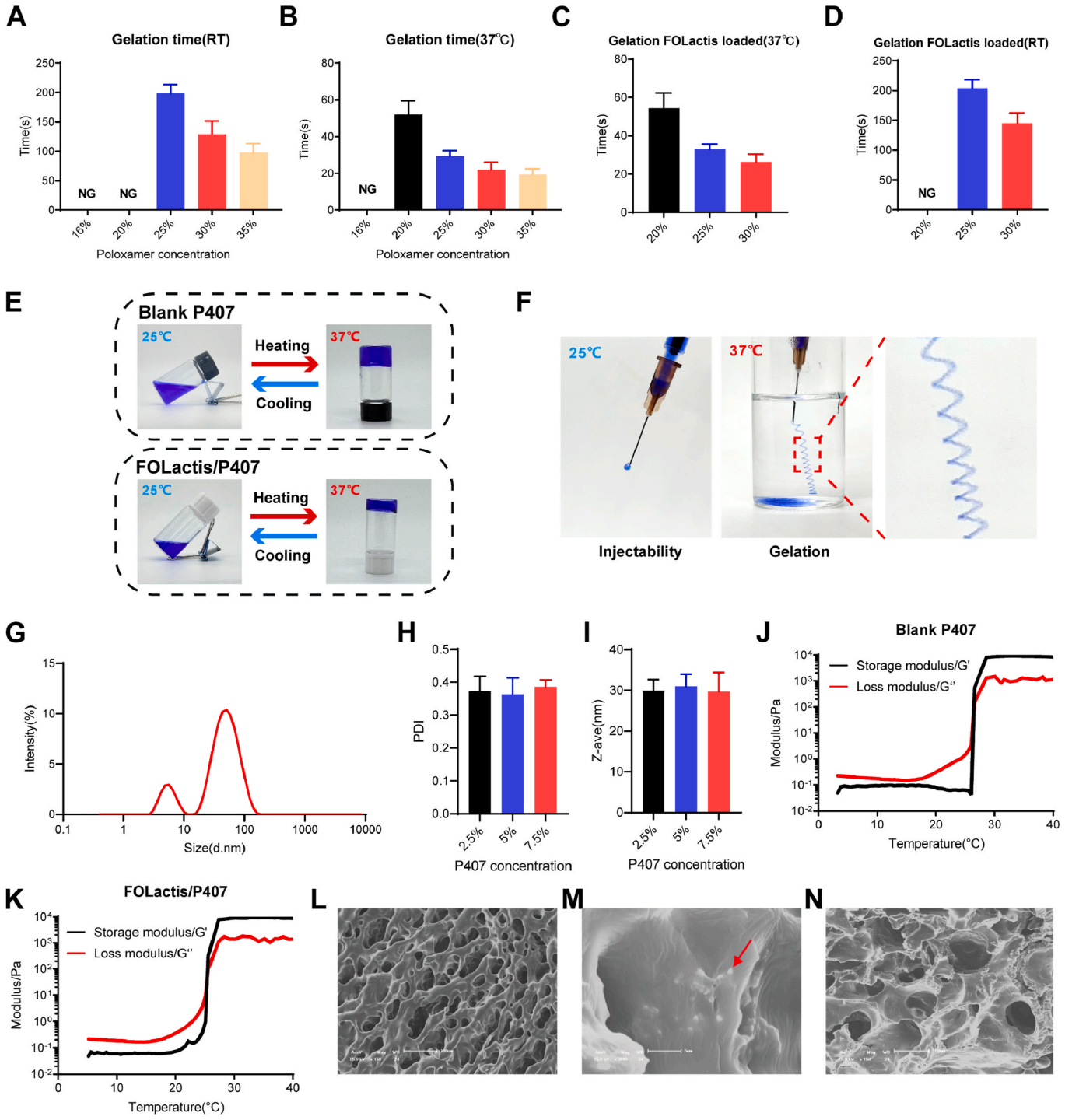

Fig. 1. Preparation and characterization of poloxamer 407 hydrogel. A-D) Time to gelation under different conditions. A) Blank P407 gel at RT. B. Blank P407 gel at 37 °C. FOLactis loaded P407 at RT. D. FOLactis loaded P407 at 37 °C. FOLactis loading amount: 5×10^9 CFU mL^{-1}. Time was measured through waterbath, and 1 mL of hydrogel was pipetted up and down with 1 mL tips until the tip became clogged. When fluidic hydrogels reach this point, keep track of the time as 'Time to gelation'. E) Reversible sol-gel phase transition of blank P407 hydrogel (20 wt%) and FOLactis/P407 hydrogel (FOLactis loading amount:5×10^9 CFU mL^{-1}) between 25 and 37 °C. F) The injectability and gelation/micelle of FOLactis/P407 hydrogel. G) The representative histogram for the micelle (5 wt%) via dynamic light scattering. H–I) The PDI and average size (z-ave) of hydrogel micelle. The error bars represented mean ± SEM for triplicate measurement. J) Changes in storage modules (G′) and loss modulus (G″) of blank P407 hydrogel (20 wt%) as a function of temperature. K) Changes in storage modules (G′) and loss modulus (G″) of FOLactis loaded P407 hydrogel (20 wt%) as a function of temperature. FOLactis loading amount: 5×10^9 CFU mL^{-1}) Scanning electron microscope images of blank P407 hydrogel (20 wt%, scale bar is 100 μm) M) FOLactis loaded P407 hydrogel and representative images of FOLactis in P407 hydrogel (Manifested by the arrows, the scale bar is 5 μm) N) SEM images of blank P407 hydrogel (16 wt%, scale bar is 100 μm).

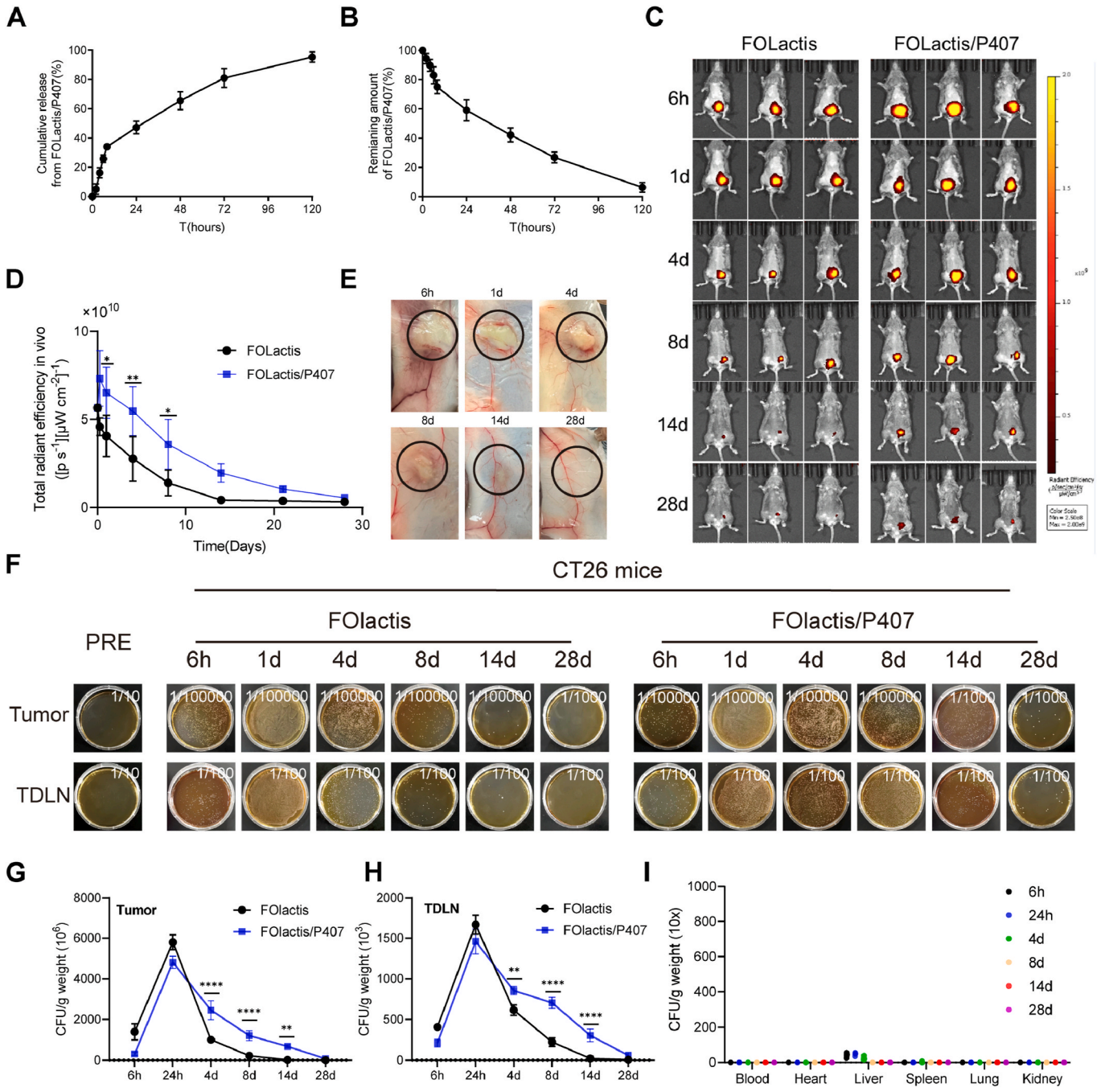

Fig. 2. FOLactis release from poloxamer 407 hydrogel in vitro and vivo. A) FOLactis release from 20% P407 hydrogel. FOLactis loading amount: 5×10^9 CFU/mL. The error bars mean ± SEM for 3 independent experiments, $n = 3$ respectively. B) Degradation of FOLactis loaded 20% P407 hydrogel in A. C) Near-infrared (NIR) imaging of male C57BL/6 mice on 6 h, 1 day, 4 days, 8 days, 14 days and 28 days after subcutaneous injection with FOLactis (5×10^9 CFU in 100 μl normal saline) or FOLactis/P407 (5×10^9 CFU in 100 μl 20% P407 solution) ($n = 3$). Ahead of injection, FOLactis were dyed with DIR (5 μM). D) Total radiant efficiency in vivo of C57BL/6 mice after injection with FOLactis or FOlactis/P407 over time ($n = 3$). The error bars represented mean ± SEM. p-values were calculated by two-way ANOVA and Tukey post-test and correction. * represented $p < 0.05$ and ** represented $p < 0.01$. E) Represent images of FOLactis loaded P407 hydrogel for 6 h, 24 h, 4 days, 8 days, 14 days and 28 days after subcutaneous injection in vivo. F) Representative images of tumors and TDLNs on solid GM17 agar plates through bacterial colonization. G-I) Quantification of bacterial colonization in tumors (G), TDLNs (H)and major organs (I) harvested from CT26-bearing mice at indicated time points after peritumoral injection of FOLactis or FOLactis/P407. The error bars represented mean ± SEM ($n = 3$, biologically independent samples). p-values were calculated by two-way ANOVA and Tukey post-test and correction. ** represented $p < 0.01$ and **** represented $p < 0.0001$.

in PBS).

In our design, FOLactis are mixed with P407 hydrogel before gelation and then distributed in micelles uniformly at room temperature. When exposed to body temperature, prompt gelation will load FOLactis, which would be profitable to stable existence of bacteria in the hydrogel for longer time. To detect the slow release of FOLactis from P407 hydrogel, Near-infrared fluorescence imaging (NIR) was employed after subcutaneous injection of P407 hydrogel loaded with DIR-stained FOLactis. As shown in Fig. 2C and D, the P407 hydrogel extends the time of releasement and depletion of FOLactis in situ after administration. For FOLactis/P407, 55% fluorescence intensity remained 5 days after injection while only 27% remained in the pure FOLactis. The

contrast became 19.6%–0.5% after 14 days. As reported previously [15], FOLactis had outstanding effect to recruit and activate DCs. We have reasons to consider that FOLactis would recruit and activate DCs for at least 14 days when encapsulated in P407 hydrogels. Furthermore, we observed the degradation of hydrogel in subcutaneous tissue over time. 5×10^9 CFU FOLactis were loaded into 20 wt% P407 before injection and hydrogel gelated within few seconds once exposed to body temperature. Then we observe the hydrogel at indicated times until degraded totally. What is remarkable is that mild local inflammation was observed in the beginning 1–2 days after injection, like rubor, calor, even slight ulceration. The hydrogel degraded utterly after about 28 days (Fig. 2E).

Moreover, we assessed the biodistribution of FOLactis/P407 at different time points after peritumoral injection by bacterial colonization, compared with pure FOLactis. It showed that FOLactis and FOLactis/P407 bacteria growth was mainly restricted to treated tumors and TDLNs (Fig. 2F). At initial time points, pure FOLactis exhibit higher concentration in tumors (1.4×10^9 CFU g^{-1} at 6 h and 5.8×10^9 CFU g^{-1} at 24 h) and TDLNs (4.1×10^5 CFU g^{-1} at 6 h and 1.6×10^6 CFU g^{-1} at 24 h) possibly due to prompt distribution when dissolved in NS, compared to FOLactis in tumor (3.1×10^8 CFU g^{-1} at 6 h and 4.8×10^9 CFU g^{-1} at 24 h) and TDLNs (2.1×10^5 CFU g^{-1} at 6 h and 1.4×10^6 CFU g^{-1} at 24 h). However, conditions remarkably altered as time went on, more FOLactis were found in tumors and TDLNs for 4 days till 28 days, with complete degradation of FOLactis/P407. On day 8, the contrast became 1.2×10^9 CFU g^{-1} to 2×10^8 CFU g^{-1} in the tumor and 7×10^5 CFU g^{-1} to 2.2×10^5 CFU g^{-1} in TDLNs (Fig. 2G and H). Besides, bacteria growth mainly remained restricted to treated tumors and TDLNs, only bare bacteria could be cultured from liver at initial time points, and the amount became fewer when loading into P407 hydrogel (Fig. 2I and Fig. S3, Supporting Information). Overall, prolonged metabolism and survival were found in FOLactis loading into P407 hydrogel, meaning more sustained immunity stimulation such as DC recruitment and activation.

2.3. Biodistribution and DC activation of FOLactis/P407

In our previous study [15], intratumoral injection of 1×10^9 CFU FOLactis proved effect and reside for about 10 days. However, biodistribution is unknown when more bacteria load into P407 hydrogel and administrated peritumorally. To identify the bacterial motility in vivo, 1×10^{10} DIR-labeled pure FOLactis or FOLactis/P407 were peritumorally injected once to visualize the distribution of FOLactis by NIR imaging. It is worth noticing that all injected pure bacteria were mainly trapped in the edge and core of the tumor and TDLNs, which peaked at 24 h and sustained for nearly 14 days after treatment. By contrast, bacteria peaked at 4 days. They remained for about 28 days after loaded into the hydrogel, signifying higher and more sustained bacterial concentrations focused on tumor and TDLNs, being beneficial to immune infiltration and functioning as a lymph island (Fig. 3A). Besides, we resected tumors and TDLNs for measurement and quantitation ex vivo at indicated time points (Fig. 3B and C). For pure FOLactis, the signal was detected at 6 h strongly in tumors and TDLNs and sustained for about 10 days, while the signal of DIR-labeled FOLactis/P407 was detected at 6 h, lasting for approximately 28 days. On day 8, almost 2 times more FOLactis were found in tumors when loading into hydrogel than pure FOLactis. What is more, continuation of high signals was measured in FOLactis/P407, which might provide an excellent opportunity for immune activation in tumors and TDLNs (Fig. 3D and E). In addition, there was almost no fluorescent signal in other organs in neither pure FOLactis nor FOLactis/P407, including the heart, liver, spleen, lung, and kidney, which means peri-tumor injection also leads to restriction of FOLactis with good biological safety (Fig. S4, Supporting Information).

The function of recruiting and activating DCs of Flt3L, together with OX40L, had been widely reported [39], which is also indicated in our previous research [15]. To detect the relationship between the number of DCs recruited and the amounts of FOLactis, 20 wt% FOLactis/P407 hydrogel were subcutaneously injected to form hydrogels, then taken out on the 1st, 3rd, and 7th days, respectively, for cell counting and flow cytometry analysis. As time went by, the total number of cells increased with the increasing amounts of FOLactis. For example, nearly 7×10^9 total cells were recruited by 1×10^{10} CFU FOLactis on 3 days, among which 11.5% were DCs, while only 4×10^5 total cells were detected in blank hydrogel (Fig. 3F and G). It should be noted that the proportion of DCs cannot fully reflect the recruitment capacity of FOLactis due to the difference in the total number of cells. The numbers of DCs recruited by 1×10^{10} CFU and 1.5×10^{10} CFU were similar on 3 days (8×10^5 DCs vs 9.8×10^5 DCs). Compared to blank P407, the addition of FOLactis significantly enhanced the number of DCs at various amounts (Fig. 3H). Then, we detected the proportion of activated DCs induced by FOLactis/P407 hydrogel in vivo. Hydrogels were taken out to harvest all cells for flow cytometry analysis on day 3 after injection. As shown in Fig. 3I, the proportion of $CD80^+CD86^+$ DC cells enhanced markedly due to FOLactis/P407, with 14.7% in 5×10^9 CFU, 17.4% in 1×10^{10} CFU, and 18.9% in 1.5×10^{10} CFU respectively. Besides, increasement of $CD103^+$DCs was also detected (Fig. 3J), meaning sustained release FOLactis from in situ hydrogel. Considering the high amounts of bacteria may induce unclear local and system inflammation and side effects, we tend to choose 1×10^{10} CFU loading into P407 hydrogel in the following study. Overall, in situ FOLactis/P407 hydrogel shows the vigoroso capacity to recruit DCs at different concentrations over time.

2.4. Antitumor effect of FOLactis/P407 in subcutaneous model

Firstly, to optimize the amount of FOLactis encapsulated in P407 hydrogel, dose-effect relationships were detected through a subcutaneous model (Fig. S5A, Supporting Information). The mice were randomly separated into 4 groups, including 5×10^9 FOLactis, 5×10^9 FOLactis/P407, 1×10^{10} FOLactis, and 1×10^{10} FOLactis/P407. Then FOLactis were dissolved in 100 μl NS or 20 wt% P407 and treated mice through subcutaneous peritumoral injection. The tumor volume and body were monitored every 2–3 days till termination. 5×10^9 CFU FOLactis show less tumor suppress effect than 1×10^{10} CFU Lactis either in NS or P407 hydrogel (Fig. S5B, Supporting Information). In addition, more amount of FOLactis lead to more prolonged survival of treated mice (Fig. S5D, Supporting Information). Taking the efficacy and side effects into consideration, 1×10^{10} CFU FOLactis were used for the following experiment.

In order to estimate the antitumor effect of in situ FOLactis/P407 in vivo, a CT26 mouse colon cancer subcutaneous model was established in male Balb/c mice and received treatment at indicated time points via peritumoral injection (Fig. 4A). When tumor volume reached about 100 mm^3, the mice were randomly separated into 5 groups, including NS, P407, Lactis, FOLactis, and FOLactis/P407. Then 1×10^{10} CFU Lactis or 1×10^{10} CFU FOLactis were dissolved in 100 μl NS or 20 wt%P407 and treat mice through subcutaneous peritumoral injection. The tumor volume, body weight, and temperature of mice were monitored every 2–3 days till termination. As shown in Fig. 4B and C, tumors in NS and P407 groups grew promptly, while tumor growth of the FOLactis and FOLactis/P407 groups were inhibited significantly, among which FOLactis/P407 treatment controlled the growth of tumors to the utmost extent. Tumors in the Lactis group grew slower slightly, probably due to the intrinsic antitumor effects of bacteria. Fig. 4D demonstrates tumor growth of each mouse in all groups, among which half of the mice grew slowly in FOLactis/P407 groups, whose volume remains below 150 mm^3 all the time. What is more, simultaneous and effective inhibition of tumors by in situ hydrogel also leads to similar results in survival curves. Mice in the NS and P407 groups all died within 40 days, similar to the Lactis group for about 41 days. 33% (2/6) of mice in the FOLactis group survived for 60 days, which extended to 83% (5/6) significantly in the FOLactis/P407 group (Fig. 4G).

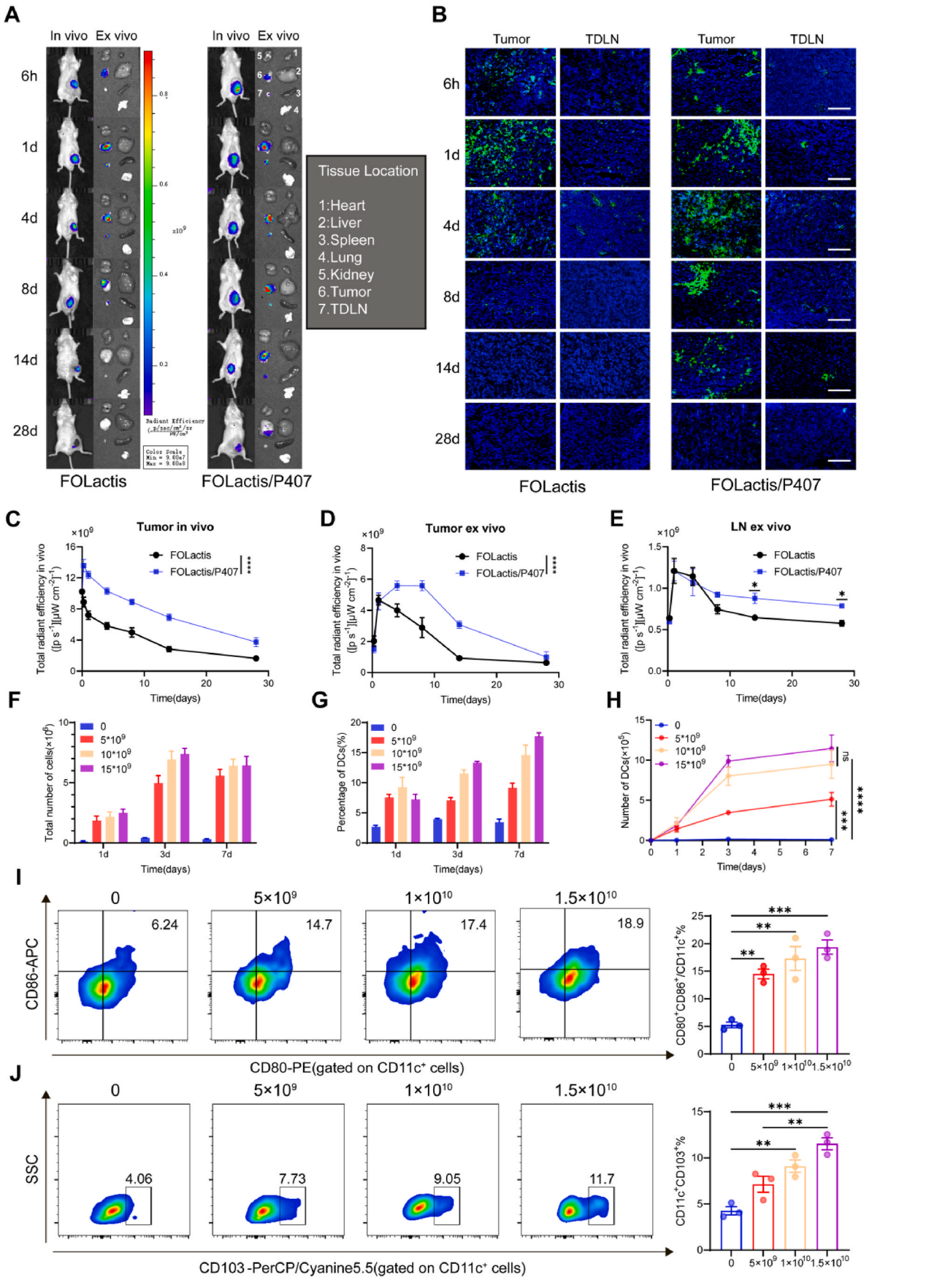

(caption on next page)

Fig. 3. Biodistribution and capacity to recruit DCs from FOLactis/P407. A) Representative NIR imaging of tumor-bearing male Balb/c mice at indicated times in vivo and ex vivo. For ex vivo images, hearts, livers, spleens, lungs, kidneys, tumors and TDLNs were harvested after FOLactis or FOLactis/P407 peritumoral injection. FOLactis loading amounts were 5×10^9 CFU/per mouse and dyed with DIR (5 μM) before injection. P407 concentration was 20%. B) Frozen sections of tumors and TDLNs in CT26 mouse colon tumor model at different times after peritumoral injection of FOLactis or FOLactis/P407 ($n = 3$). FOLactis were labeled with DiO (green); nucleus, blue. Scale bars is 100 μm. C-D) Total radiant efficiency of FOLactis and FOLactis/P407 in tumors in vivo (C) and ex vivo (D) along with time. The error bars represented mean ± SEM ($n = 3$, biologically independent samples). E) Total radiant efficiency of FOLactis or FOLactis/P407 in TDLNs ex vivo along with time. The error bars represented mean ± SEM ($n = 3$, biologically independent samples). F-G) Total number of cells (F) and percentage of DC cells (G) on 1st, 3rd and 7th days in P407 hydrogel loaded with 4 different concentrations of FOLactis. H) Number of DCs in 1 week from P407 hydrogel loaded with 4 different concentrations of FOLactis. I-J) Representative flow plots and flow cytometric analysis of $CD11C^+CD103^+$ DCs (I) and $CD80^+CD86^+$mDCs gated on $CD11c^+$ DCs (J). For the flow cytometric analysis in F-J, the error bars represented mean ± SEM ($n = 3$). Statistical significance was determined by analysis of *p*-values were calculated by two-way ANOVA (C,D,E,H) and two-tailed unpaired Student's t-tests (I,J). * represented $p < 0.05$, ** represented $p < 0.01$, *** represented $p < 0.001$ and **** represented $p < 0.0001$.

2.5. Immune response induced by in situ FOLactis/P407 hydrogel in vivo

To gain mechanistic insight into the local and systemic immunological responses induced by in situ FOLactis/P407 hydrogel, tumor suppression experiment above was repeated. On 4 days after last peritumoral treatment, tumors, TDLNs, and spleens were harvested to detect the changes in immune populations by flow cytometry. There was almost no difference between NS and P407 groups in all immune populations detected, illustrating no antitumor effect and immune response induced by P407 hydrogel inherently. As shown in Fig. 5A–G, the proportions of $CD103^+$DCs from tumors increased in the last 3 groups (Lactis, FOLactis, and FOLactis/P407), among which FOLactis/P407 group was the highest and had about 3 times increasement compared to NS group. The ratio of effective T cells ($CD3^+CD8^+$) also increased from tumors in FOLactis/P407 groups (14%) in contrast to FOLactis (11%) and the rest groups (Fig. 5D). As we know, TDLNs are essential for tumor antigen-loaded DCs to activate naïve T cells. As shown in Fig. 5B–E, the 'lymph island' formed by FOLactis/P407 reinforced the ISV effect of FOLactis and induced a large number of mature DCs in TDLNs for long time. The upregulation of $CD80^+CD86^+$ ratio proved more mature stage of DCs, among which the functional $CD103^+$DCs also had increased compared to the other groups (Fig. 5F).

Then we detected the proportion of effector memory T cells (T_{EM}, $CD3^+CD8^+CD44^+CD62L^-$) because of its important role in secreting cytokines to kill tumor cells. The proportion of T_{EM} in the NS and 407 were 33.8% and 36.8%, which were lower than the other 3 groups, among which the highest proportion of T_{EM} was 70.3% in the FOLactis group (Fig. 5C and I). It was worth mentioning the proportion of T_{CM} ($CD3^+CD8^+CD44^+CD62L^+$) in the FOLactis group (12.7%) was significantly lower than FOLactis/P407 (20.5%) while Lactis was basically at the same level, indicating the essential role of in situ P407 hydrogel to inducing long-term immune response with the hydrogel (Fig. 5C–H).

Over and above the infiltration of various DCs and T cells in the tumors, TDLNs, and spleens, we also investigated NK cells and tumor-associated macrophages (TAMs), which played important roles in innate immunity. NK cells were similar in NS and P407 groups, with an average ratio of 7.9% and 8.8%. In comparison, the other 3 groups were 11.0% (Lactis), 16.6% (FOLactis) and 20.4% (FOLactis/P407) respectively, indicating contribution of FOLactis to increasing NK cells which further improved through P407 hydrogel (Figs. S6A and C, Supporting Information). Besides, both Lactis and FOLactis polarized TAMs from immunosuppressive type 2 macrophages (M2, $CD11b^+F4/80^+CD206^+$) to immune promoting type 1macrophages (M1, $CD11b^+F4/80^+CD86^+$) slightly. Compared to the NS group (3.1%) and P407 group (3.2%), the proportion of M1 in the Lactis and FOLactis groups increased to 3.9% and 6.5%. In situ FOLactis/P407 maximized their synergy, reaching 9.1% in M1, the highest in all groups (Figs. S6E and F, Supporting Information). What is more, we detected the PD-1 expression from tumor and PD-1 on $CD4^+$ T cells were significantly increased in FOLactis/P407 group (50.3%), reaching about 5 times compared to the NS group (12.2%) and P407 group (12.6%) (Figs. S6B and D, Supporting Information).

Besides, CT26 tumors were collected 4 days after the last treatment to evaluate the therapeutic efficacy of this local immunotherapy by immunohistochemical analysis. The number of $CD8^+$ T cells and $CD11c^+$ DC cells significantly increased after peritumoral injection of FOLactis, and FOLactis/P407 further strengthen immune infiltration in TME (Figs. S6G and H, Supporting Information).

The results gave adequate explanations of the best tumor suppression effect in the FOLactis/P407 group since the disadvantages in other groups. Firstly, the P407 hydrogel itself has almost no effect on induction of immune cells. Secondly, the Lactis group could only regulate immunity innately through lysates in the absence of Flt3L and OX40 fusion protein. In addition, FOLactis group contained all antitumor drugs, but without the slow release of the in situ hydrogel, these drugs were metabolized too quickly in vivo that there was not enough time for them to exert antitumor effects, proving the importance of a suitable drug carrier functioning as lymph island. Besides, increasement in the expression of PD-L1 on tumor cells implied a good synergistic effect between the in situ FOLactis/P407 hydrogel and the PD-1 antibody (aPD-1).

2.6. FOLactis/P407 treatment reduces tumor burden expressively over time in abdominal metastasis mouse models

To further detect the efficacy of in situ FOLactis/P407 hydrogel in the mouse model of abdominal metastasis, 5–6 week Balb/c male mice were inoculated with 5×10^5 CT26 mouse colon cells intraperitoneally on day 0. CT26 tumors exhibit a high mutational load, are highly immunogenic, and are amenable to many immunotherapy approaches. Then we randomly divided mice into 5 groups 7 days after inoculation: NS, P407, Lactis, FOLactis, and FOLactis/P407 and treated every 7 days until termination (Fig. 6A). On the 27 days of treatment, tumor nodules reduced dramatically in the abdominal cavity from in situ FOLactis/P407 group (Fig. S7, Supporting Information). Then we harvested and weighed tumor tissues 6 days after last administration (Fig. 6B). The tumor tissues from NS and P407 groups were similar and heavier than the other 3 groups. Among all groups, tumor tissue harvested from the FOLactis/P407 group (868 g) appeared different in color and vascularity. It weighed nearly 6 times less than the NS and P407 group (5381 g and 4996 g) (Fig. 6C). Although the average body weight of the mice in each group was not similar due to large amount of bacteria intraperitoneal administration, there was still a significant difference in the tumor/body weight percent of the tumors collected from the mice (Fig. 6D).

Besides, malignant abdominal ascites harvested from FOLactis and FOLactis/P407 group did not appear similar in volume nor color to the other 3 groups (Fig. 6E). Lactis group (1836 μl) showed slight inhibition in ascites formation compared to NS and 407 groups (2626 μl and 2445 μl), while average ascites in FOLactis group were 411 μl. It is worth mentioning that the volume of malignant abdominal ascites from FOLactis/P407 group was only 129 μl, the fewest, and more than 3 times less than the FOLactis group, let alone other groups (Fig. 6F). For survival study, all mice in the FOLactis/P407 group were alive until endpoints of monitoring therapy. In contrast, 66% of mice FOLactis group died before 60 days, and no mice lived more than 40 days in the other 3

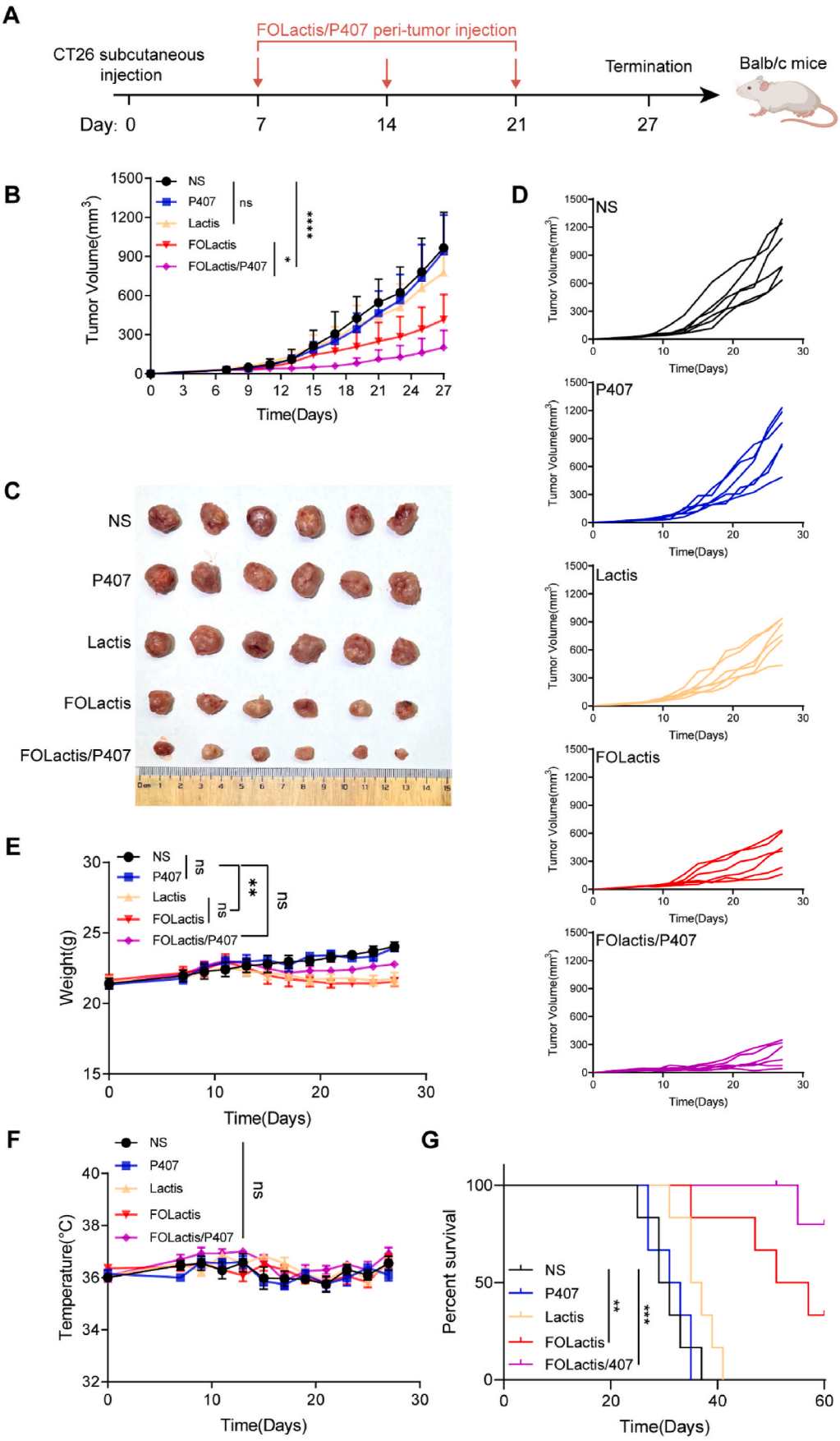

(caption on next page)

Fig. 4. Antitumor effect of FOLactis/P407 in subcutaneous model. A) Schematic diagram of administration of FOLactis/P407 in CT26 tumor-bearing mice. 1×10^6 cells were injected subcutaneously on the right lower sides of the abdomen to establish CT26 tumor model. B) Average tumor-growth curves of BALB/c mice bearing CT26 tumor with different treatments as indicated. The mice were peritumorally injected with NS, P407,1×10^{10} Lactis, 1×10^{10} FOLactis or 1×10^{10} FOLactis/P407, which were dissolved to a final volume of 100 μl per dose when tumor volume reached about 100 mm^3. P407 concentration was 20%. Tumor size was measured every 2–3 days for 27 days. The error bars represented mean ± SEM ($n = 6$). *p*-values were calculated by two-way ANOVA and Tukey post-test and correction. ns represented $p > 0.05$, * represented $p < 0.05$ and **** represented $p < 0.0001$. C) Photos of tumors harvested from Balb/c mice in all groups on the 25th day after tumor inoculation ($n = 6$). D) Average weight of different groups for 27 days. The error bars represented mean ± SEM ($n = 6$). *p*-values were calculated by two-tailed unpaired Student's t-tests. ** represented $p < 0.01$. E) Tumor-growth curves of each mouse in different groups ($n = 6$). F) Average temperature of each mouse in different groups for 27 days. The error bars represented mean ± SEM ($n = 6$). *p*-values were calculated by two-tailed unpaired Student's t-tests. ns represented $p > 0.05$. G) Survival curves of different groups for 60 days. The error bars represented mean ± SEM ($n = 6$). *p*-values were calculated by log-rank (Mantel–Cox) test, * represented $p < 0.05$.

groups (Fig. 6I). Overall, the work described above illustrated in situ P407 hydrogel enhanced the tumor suppression efficacy of FOLactis ulteriorly through prolonged releasement and adherence to abdominal metastasis tumors.

2.7. Antitumor effect of FOLactis/P407 in orthotopic gastric mouse models

Given the good adherence of in situ P407 hydrogel, we hypothesize FOLactis/P407 could cling to tumor nodules and organs like stomach, functioning as a lymph island and suppressed locally advanced gastric tumors. To establish orthotopic gastric mouse model, 5×10^5 MFC/MFC-Luc cells suspended in 50 μl NS were injected into the stomach wall of 6–8 week male 615 mice. 7 days after inoculation, mice were randomly divided into 5 groups: NS, P407, Lactis, FOLactis and FOLactis/P407. 7 days later, drugs indicated were administered intraperitoneally 3 times in 2 weeks (Fig. 7A). It deserves to mention NIR imaging was employed to detect tumor location before treatment to ensure peritumoral injection. As shown in Fig. 7B and C, tumor-bearing stomach resected from mice in FOLactis and FOLactis/P407 groups were not similar with other 3 groups in size of orthotopic tumor. Tumors in all groups caused severe mass effects except the FOLactis/P407 group. The average weight of orthotopic tumor in the FOLactis group (183 mg) were about 3 times less than NS group (659 mg) and P407 group (621 mg), the weight decreased to 27 mg when loading FOLactis into in situ P407 hydrogel. Besides, abdominal metastasis tumor nodules were also collected to evaluate tumor burden. Only average 3 tumor nodules were found in the abdominal cavity of the FOLactis/P407 group, while 16 tumor nodules in the FOLactis group, let alone at least 30 tumor nodules in the NS, P407, and Lactis group (Fig. 7D).

Moreover, NIR imaging was used to detect MFC-Luc tumor burden dynamically, the total flux from the Lactis group dropped slightly, mainly due to innate immunity. Both FOLactis and FOLactis/P407 group declined significantly till 14 days. Total flux from the FOLactis group turned to enhance while FOLactis/P407 group went on dropped to nearly CR (Complete Remission) (Fig. 7G and H). The survival curves had similar results (Fig. 7I). Mice in NS and P407 groups died within about 30 days after tumor inoculation, and the survival rate of FOLactis/P407 was 83.3% (5/6) till observed endpoints, better than 50% (3/6) in the FOLactis group. The results above proved our hypothesis that in situ P407 hydrogel, while loading drugs like FOLactis, could persistently eradicate orthotopic gastric cancer in mouse model.

2.8. Biosafety of FOLactis/P407 hydrogel

For translational application, it is essential to assess the biosafety of FOLactis/P407. Firstly, the cytotoxicity of blank P407 hydrogel was evaluated through CCK8(cell counting kit-8). CT26 and MFC mouse cancer cells were co-incubated with different concentrations of P407, and then cell viability was detected at indicated time points. Cell viability in CT26 cells, as well as MFC cells, did not show significant decrease over time for any concentrations up to 10%, meaning P407 hydrogel is biocompatible and does not exert tumoricidal effects by itself (Figs. S1E and F, Supporting Information). For in vivo experiments, mice in pure Lactis and FOLactis group experienced about 10% weight reduction during treatment over time, especially in intracavitary injection (Figs. 4E, 6G and 7E). Mice in the FOLactis/P407 group could gain less weight reduction because of in situ slow release and barrier effect. We believed that compared to the FOLactis/P407 group, mass Lactis/FOLactis bursted in a short time and caused weight loss. The mice in all groups did not experience abnormal temperature fluctuations over time (Figs. 4F, 6H and 7F).

In addition, systemic inflammation and hepatorenal function of mice in each group were also detected. No significant changes were observed in aspartate aminotransferase (AST), alanine aminotransferase (ALT), alkaline phosphatase (ALP), blood urine nitrogen (BUN), and creatinine (CREA) in serum harvested from all groups 4 days after last treatment, which were also at the same level basically. Besides, no evident damage was detected in HE staining of main organs (heart, liver, spleen, lung, and kidney) collected from mice in different groups 4 days after the last treatment (Fig. S8, Supporting Information). For intraperitoneal metastatic tumor model, there were no significant abnormalities in blood biochemical parameters after each dose. The organs that may be involved through intraperitoneal administration did not show significant damage, such as bowel, bladder and testis (Fig. S9, Supporting Information). Cytokine storm was the most life-threatening side effects may occur during immunotherapy. The concentration of chemokines and inflammatory cytokines were detected in the serum of treated mice collected 4 days after last administration to assess systemic inflammation induced by FOLactis/P407. The serum concentration of IFN-γ, IL-5, TNF-α, IL-2, IL-6, IL-4, IL-10 and IL-13 were similar among all groups generally with no statistical significance (Fig. S10, Supporting Information).

In summary, the in situ injectable thermo-sensitive P407 hydrogel exhibit not only outstanding biosafety itself but also relieve inflammation and other side effect caused by a large number of bacteria through entrapment.

3. Discussion

Here we design a bacteria delivery system based on in situ poloxamer 407 hydrogels to enhance immunotherapy and inhibit tumor regression in the long term by rejuvenating DCs and cytotoxic T cells. Our team designed engineered *Lactococcus lactis* secreting Flt3L and OX40L fusion protein, which acted as in situ vaccination and modulate key components of antitumor immune response by intratumoral injection previously [15]. Nevertheless, in solid tumors with firm texture or high internal pressure, intratumoral injection is challenging. Moreover, intratumoral injection is not feasible in metastatic tumors like abdominal and orthotopic metastatic tumors due to the lack of available lesions.

To address the aforementioned challenges, various methods of administering FOLactis have been considered. Local administration is an important option that can effectively improve the concentration of engineered therapeutic bacteria at the tumor side and reduce the potential side effects of local systemic infection [40]. As the rapid development of materials science, hydrogels have been developed for bacteria-mediated therapy, such as bacterial-promoted wound healing,

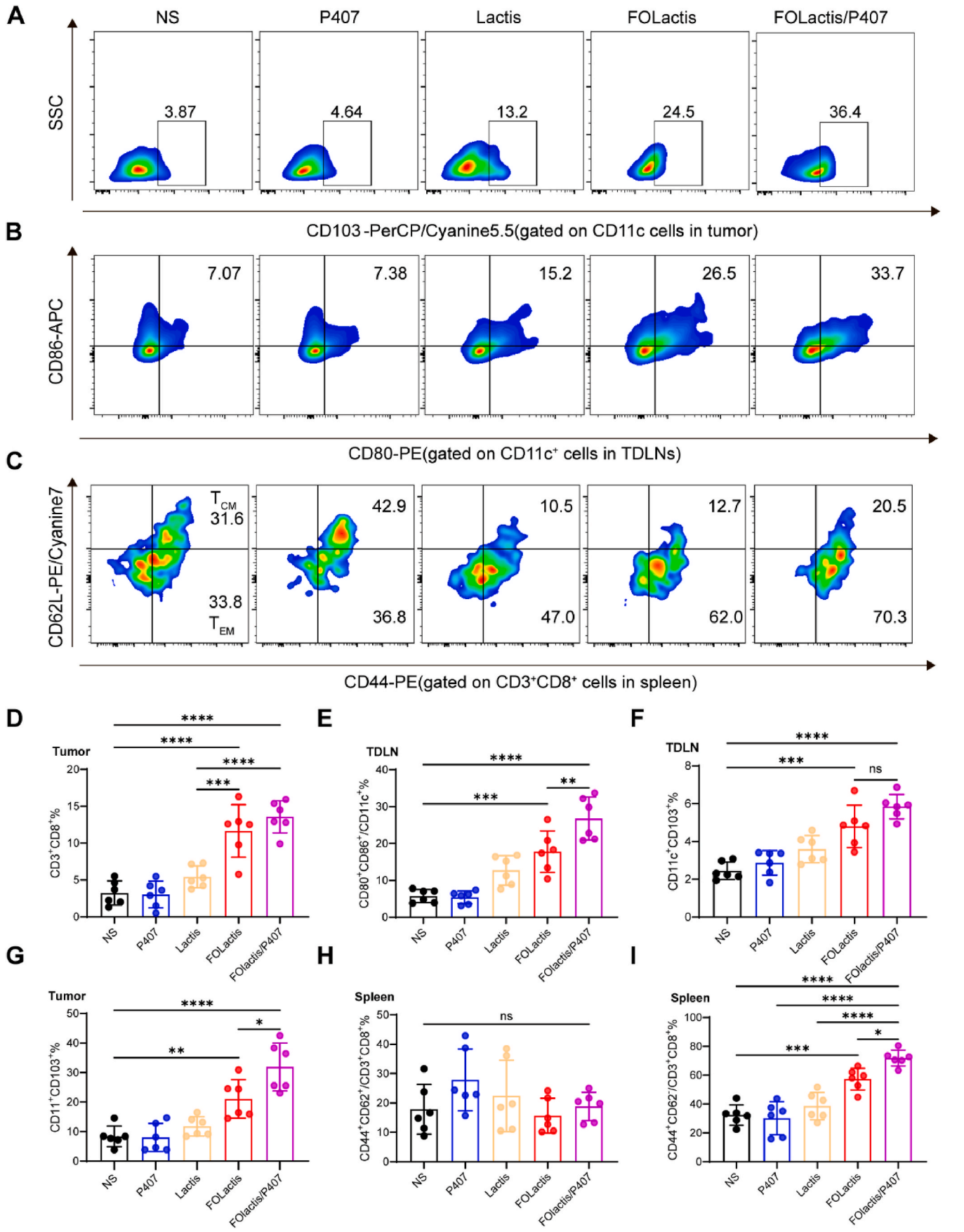

(caption on next page)

Fig. 5. FOLactis/P407 further reprogrammed the immune microenvironment in vivo. CT26 tumor-bearing mice in different groups were euthanized 4 days after the last treatment, and the proportions of immune cells were stained and analyzed by flow cytometry in the local tumor, TDLN and spleen ($n = 6$). A-C) Representative flow plots of $CD11c^+CD103^+$ (A), $CD80^+CD86^+$mDCs gated on $CD11c^+$ DCs (B) and $CD44^+CD62L^-$ T_{EM} gated on $CD3^+CD8^+$ T cells (C). Flow cytometric analysis of $CD3^+CD8^+$ T cells (D) in tumor, $CD80^+CD86^+$mDCs (E, gate: $CD11c^+$ DCs), $CD11c^+CD103^+$DCs (F) in TDLNs and $CD11c^+CD103^+$DCs (G) in tumor. H–I) Flow cytometric analysis of effector memory T cells (T_{EM}, $CD3^+CD8^+CD44^+CD62L^-$) and central memory T cells (T_{CM}, $CD3^+CD8^+CD44^+CD62L^+$) in the spleen. For the flow cytometric analysis in D-I, the error bars represented mean ± SEM ($n = 6$). Statistical significance was determined by analysis of two-tailed unpaired Student's t-tests. ns represented $p > 0.05$, * represented $p < 0.05$, ** represented $p < 0.01$, *** represented $p < 0.001$ and **** represented $p < 0.0001$.

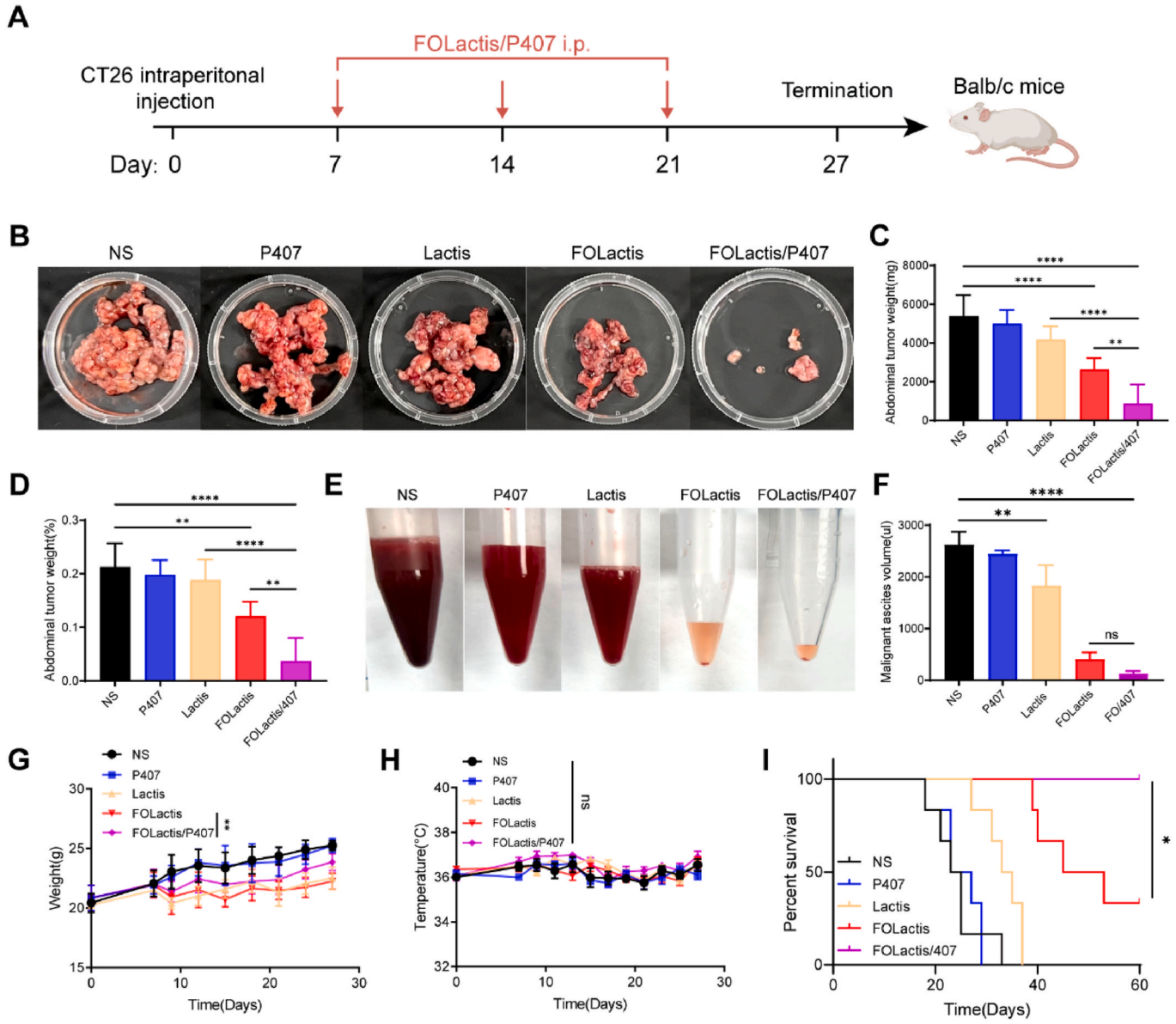

Fig. 6. FOLactis/P407 treatment reduces tumor burden expressively over time in abdominal metastasis mouse models. A) Schematic diagram of treatment of FOLactis/P407 in CT26 colon cancer peritoneal metastasis mouse models. 5×10^5 cells suspended in 200 μl NS were injected intraperitoneally on the right lower sides of the abdomen to establish CT26 colon cancer abdominal metastasis mouse model. The mice were injected intraperitoneally with NS, P407, 5×10^9 Lactis, 5×10^9 FOLactis or 5×10^9 FOLactis/P407 which were dissolved a final volume of 200 μl per dose since 7 days after inoculation. P407 concentration was 15%. The body weight and temperature were measured every 2–3 days to termination. B) Representative visible IP tumor nodules of different groups harvested and imaged 4 days after last treatment. C) Average abdominal tumor weight of different groups. D) Abdominal tumor weight as a percentage of total body weight. E) Representative malignant ascites collected and imaged 4 days after last treatment. F) Average malignant ascites of different groups. G-H) The average body weight (G) and temperature (H) of different groups. For the analysis in C-D and F–H, error bars represented mean ± SEM ($n = 6$). Statistical significance was determined by analysis of two-tailed unpaired Student's t-tests. ns represented $p > 0.05$, ** represented $p < 0.01$, and **** represented $p < 0.0001$. I. Survival curves of different groups for 60 days. The error bars represented mean ± SEM ($n = 6$). p-values were calculated by log-rank (Mantel–Cox) test, * represented $p < 0.05$.

bacterial vaccines and probiotic-mediated digestive treatment [41–43]. For cancer bacteria immunotherapy, hydrogel depots based on alginate can load engineered bioluminescent bacteria and Ce6 for self-activated PDT and systemic anticancer immunity boost [44]. Polyaldehyde dextran and chitosan viscous hydrogel has also been reported to encapsulate Exogenous P. anaerobius and synergize with PD-1 blockade

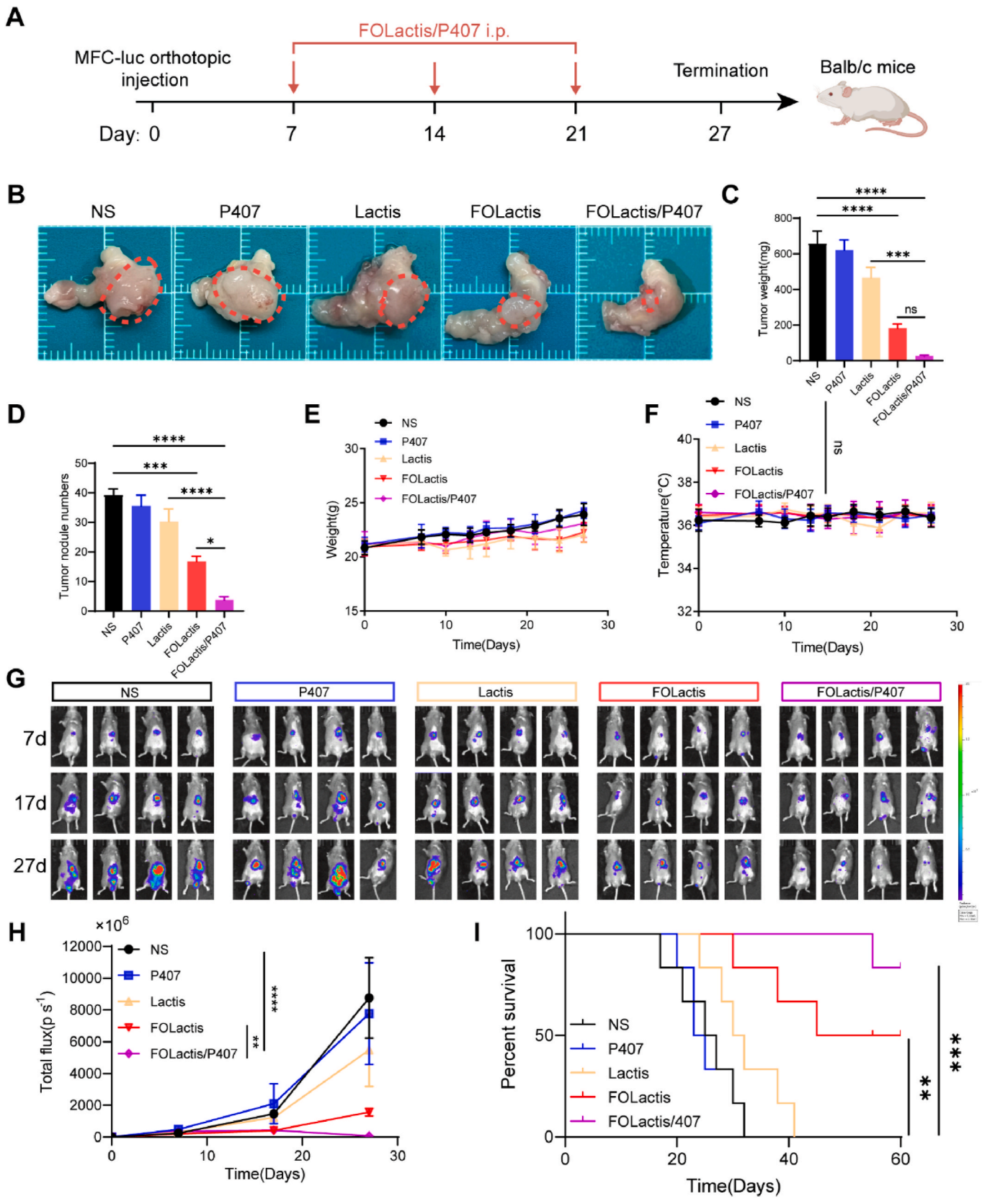

(caption on next page)

Fig. 7. Antitumor effect of FOLactis/P407 in orthotopic gastric mouse models. A) Schematic diagram of administration of FOLactis/P407 in orthotopic MFC gastric cancer mouse models. 5×10^5 cells suspended in 50 μl NS were injected into the stomach wall of 615 mice. Then the mice were injected intraperitoneally with NS, P407, 5×10^9 Lactis, 5×10^9 FOLactis or 5×10^9 FOLactis/P407 which were dissolved a final volume of 50 μl per dose 3 times in 14 days. P407 concentration was 15%. NIR was employed previously to detect the location of the tumor to ensure FOLactis/P407 was administered in the vicinity of the tumor. The body weight and temperature were measured every 2–3 days to the endpoint. B) Representative stomachs of different groups removed and imaged 2 days after last treatment. C-D) Average orthotopic tumor weight (C) and numbers of metastatic tumor nodules (D) in the abdominal cavity of different groups. E-F) The average body weight (E) and temperature (F) of different groups. For the analysis in C–F, error bars represented mean ± SEM ($n = 4$). Statistical significance was determined by analysis of two-tailed unpaired Student's t-tests. ns represented $p > 0.05$, *** represented $p < 0.001$, and **** represented $p < 0.0001$. G) Luminescent images on days 7,14 and 21 ($n = 4$). H) Tumor burden represented by total flux (photons s^{-1}) plotted on indicated times, error bars represented mean ± SEM ($n = 4$). Statistical significance was determined by analysis of two-tailed unpaired Student's t-tests. ** represented $p < 0.01$ and **** represented $p < 0.0001$. I) Survival curves of different groups for 60 days. The error bars represented mean ± SEM ($n = 6$). *p*-values were calculated by log-rank (Mantel–Cox) test, ns represented $p > 0.05$, *** represented $p < 0.001$ and **** represented $p < 0.0001$.

in mice with oral squamous cell carcinoma [45]. Hydrogels, especially formatted chemically, usually generate potential toxic agents that do harm to normal organs as well as bacteria activity. In addition, simple preparation and administration are also required for clinical translation. After many trials to test efficacy and safety, we selected poloxamer 407 as carrier to encapsulate FOLactis.

As FDA-approved polymer, the construction and biocompatibility of poloxamer 407 are proved in our study, in line with previous reports [33]. P407 were employed as carrier of microbiota-modulating agent like bacillus for skin infection treatment mainly due to its lower critical solution temperature, since it allows bacteria to grow inside the formula, prolong the retention of bacteria in the injection location without compromising bacteria's ability to produce and secret [46]. Therefore, we speculate P407 hydrogel could also prolong the preservation of FOLactis and be beneficial for secreting of fusion protein containing Flt3L and OX40L, which has been proved in follow-up experiment.

For packaging living bacteria therapy, it's essential to detect bacteria release from hydrogel since how drugs diffuse from hydrogel depends on the mesh size of hydrogel, and larger mesh usually leads to smooth release [47]. As we know, the diameter of *Lactococcus lactis* is 1.5–2.5 μm, and so is engineered FOLactis [15]. We detected the mesh size of P407 at different concentrations through SEM and finally selected 20% wt for the subsequent experiment. The release and biodistribution of FOLactis/P407 also proved that 20 wt% is the suitable concentration for FOLactis delivery.

As an important site for tumor development and metastasis, TDLNs are essential for tumor immunity, in which naïve T cells are activated to antigen-specific T_{EM} by antigen-loaded DCs [48]. However, systemic administration often fails to stimulate the immune system in TDLNs as effectively as peritumoral administration [49]. Here we innovatively proposed an approach of engineered bacteria loading in situ hydrogel by peritumoral administration. Our results indicate that FOLactis/P407 could slow the release and storage of cytokines, induce anti-tumor immune response through the interaction of T cells, DC cells and NK cells and act as an artificial lymph island, finally enhance the efficacy of FOLactis. Compared to pure FOLactis, P407 hydrogel reduces local and systemic inflammation effect significantly probably due to sustained delivery. What is more, this strategy directly provided mDCs loaded with antigens, avoiding the difficulty of enriching drugs in TDLNs and tumor microenvironment in systemic administration.

Abdominal metastasis is usually occurred in advanced gastrointestinal and ovarian tumors, meaning massive tumor burden and poor prognosis. Systemic treatment like chemotherapy is less effective due to low drug utilization rate with the risk of damage to the other normal tissues. FOLactis/P407 can inhibited tumor burden in abdominal metastasis mouse model successfully. Compared to normal saline, P407 hydrogel can distributed to abdominal cavity tardily after administration. What's more, P407 hydrogel aids in the colonization of FOLactis on the tumor nodules and relieves the potential side effect caused by FOLactis. As we know, this is the first report of using probiotics loading hydrogel via intraperitoneal injection to treat peritoneal metastatic tumors.

Surgical resection, especially D2 dissection is still the preferred choice for locally advanced gastric cancer treatment [50]. Nevertheless, local recurrence and unresectable tumors restricted the application of surgical. Thus, drug delivery systems like hydrogels and nanoparticles draw great interest to researchers [51]. Here we designed FOLactis/P407 for adjuvant combination immunotherapy of locally advanced gastric cancer. After located tumor through NIR, FOLactis were administrated near the stomach via intraperitoneal injection and suppressed tumor growth significantly for a long-time. It is mainly attributed to outstanding adherence and slow-release effect of P407 hydrogel. For clinical application, there will be more accurate and efficient approach to administrate FOLactis/P407 such as ultrasound-guided injection.

There were still some limitations in our study. The relatively high gelation concentration and low mechanical strength, which is the common failing of physical hydrogels, are not beneficial for long-term bacteria survival. It is possible to enhance the mechanical strength through adding biocompatible components like gelatin or chitosan. Besides, it is necessary to mention that the concentration of P407 for cavity injection was different from subcutaneous injection since high concentration may lead to adherence to normal organs like intestinal canal, which may lead to potential damage. Another disadvantage is that Flt3L and OX40L secreted from FOLactis are both adjuvant and need to produce immune response via recruitment and maturation of DCs as well as antigen presentation. To initiate tumor specific immune response, we also plan to recruit T cells directly by expressing antigens on surface of bacteria through synthetic biology. What is more, it makes sense for us to further research the mode of action of FOLactis/P407, such as abscopal effect, antigen-specific therapeutic effects and synergistic effects with other therapies such as radiotherapy and immune checkpoint inhibitors. In addition, single-cell transcriptomic may be implemented to analyze differences at the genetic level and revealed the development and metabolism of tumors entirely.

4. Conclusion

In this study, we creatively put forward an injectable in situ temperature-sensitive hydrogel system for engineered Lactococcus lactis delivery. The FOLactis/P407 exhibit sol-gel transition when exposed to physiological temperature and prolong drug release. DCs were proven recruited to hydrogel not only in numbers but also in activated ratios. Peritumoral injection of FOLactis/P407 greatly promotes maturation and $CD103^+$ proportion of DCs in TDLNs, induces competent T_{EM} in spleen, $CD8^+$ T cells proliferation, polarizes macrophages to M1 subtype and increases NK cells in TME, acting as artificial lymph island. Abdominal metastasis tumor and orthotopic gastric tumor model indicated that the administration of FOLactis/P407 are in favor of local drug retention and improves the anti-tumor effect significantly. In addition, FOLactis/P407 shows outstanding biocompatibility in both vivo and vitro and can reduce potential toxicity caused by large amounts of bacteria. These discoveries demonstrated clinical translational strategies for improving the immunotherapy efficacy of engineered bacteria based on in situ hydrogel delivery system.

5. Experimental section

Materials, Bacterial strains, Cells, and Animals: Poloxamer 407 was purchased from BASF (P407/F127, Ludwigshafen, Germany). *Lactococcus lactis* NZ9000 and pNZ8148 vector were obtained from MoBiTec (Germany). *Escherichia coli* BL21 (DE3) was purchased from Shanghai Weidi Biotechnology Co, Ltd. *Escherichia coli* strains were incubated in Luria-Bertani (LB) medium at 37 °C with shaking at 220 rpm. Lactis NZ9000 was propagated statically in M17 (Oxoid) medium containing 0.5% (w/v) glucose (GM17) at 30 °C. CT26 and MFC cells were obtained from the Cell Bank of Shanghai Institute of Biochemistry and Cell Biology. CT26 colon cancer cells and MFC/MFC-GFP-Luc gastric cancer cells in Roswell Park Memorial Institute (RPMI) 1640 (Gibco) supplemented with 10% fetal calf serum, 100 U ml^{-1} penicillin, and 100 μg mL^{-1} streptomycins at 37 °C and 5% CO2. Cells were tested for Mycoplasma, and only Mycoplasma-free cells were used. BALB/c and 615 male mice aged 5–6 weeks were purchased from Shanghai Sippr-BK laboratory animal Co. Ltd. (Shanghai, China) and kept in the specific pathogen-free (SPF) Laboratory Animal Center of Affiliated Nanjing Drum Tower Hospital of Nanjing University Medical School. All mice were maintained in specific pathogen-free animal facility with controlled temperature (68–79 °F), humidity (30–70%) and light/dark cycle (lights between 6 a.m. and 6 p.m.). Feed and water were available ad libitum. All animal experimental protocols were approved by the Laboratory Animal Care and Use Committee of the Affiliated Nanjing Drum Tower Hospital of Nanjing University Medical School (2022AE01021).

Generation and characterization of Lactis and FOLactis: Generation and characterization of Lactis and FOLactis were described in our previous study in detail [15].

Preparation of hydrogel: The 'cold' method was deployed to prepare P407 hydrogels. For example, to prepare a 20% poloxamer hydrogel formulation, 2 g poloxamer powder was slowly dissolved in 10 mL normal saline and then stirred overnight at 4 °C until all of the granules were dissolved. Formulations ranging from 16% to 35% poloxamer were prepared for initial analyses. Lactis or FOLactis was then added to the gel by mixing when solutions became clear.

Characterization analysis of hydrogel: 5 mL Eppendorf tubes were kept at 20 °C or 37 °C using a waterbath, and 1 mL of hydrogel was pipetted up and down with 1 mL tips until the tip became clogged. When fluidic hydrogels reach this point, record the time as 'gelation time'. The rheometer (AR 2000ex, TA, Italy) was used for the transformation of the rheological properties with the temperature variation in oscillatory state. In addition, hydrogel preparations were located between the parallel plates (the type of the plate was 40 mm 2° steel cone, and the gap was set as 0.63 mm) and conducted with the temperature ramp test. The detection occurred in the temperature range of 10–40 °C with the strain and angular frequency were fixed as 2% and 10 rad s^{-1} respectively, the heating rate was 1 °C min^{-1}. Injectability was detected by a 24G syringe needle at room temperature. Dynamic light scattering (DLS) measurements were accomplished with a Malvern Zetasizer (Nano ZS, Malvern Ltd., UK). 2.5%, 5 and 7.5% P407 solutions were prepared, and the size, poly dispersity index (PDI), and Z-ave were measured at 20 °C. H-NMR measurements were taken with AVANCE NEO 400 M (Bruker, Germany). FTIR spectra were obtained using Spectrum Two (PerkinElmer, America) within the wavenumber range from 4000 to 500 cm^{-1}. P407 hydrogels were lyophilized and sputter coated with a gold layer. The morphology was then observed with scanning electron microscopy (SEM; SSX-550, SHIMADZU, Japan). The cytotoxicity of P407 hydrogels on CT26 and MFC/MFC-Luc cells was evaluated by cell counting kit-8 (CCK8). About 5×10^3 cells/well were planked in the 96-well plate with RMPI 1640. Then replace RMPI 1640 with different concentration of Poloxamer 407 (0.625%, 1.25%, 2.5%, 5%, 10%) after cell attachment. All culture mediums were enriched with 10% fetal calf serum, 100 U ml^{-1} penicillin, and 100 μg mL^{-1} streptomycins. After 24 h, 48 h, and 72 h of incubation, the CCK8 mixed RMPI 1640 medium was added to the cells. Wells containing medium only were included as background measurements. After 2 h, depending on the conversion rate, the sample ODs were determined with a spectrophotometer (Thermo scientific, USA) set on 490 nm. Cell viability is calculated using the following formula: (treated cells –background)/(untreated cells –background) × 100, then calculated and expressed in percentage (%).

In vitro FOLactis release: 'Membrane-less method', which was described earlier [52–54], was used to trace vitro FOLactis release. 1 mL P407 hydrogel mixed with 5×10^9 CFU FOLactis was stored at 37 °C to induce gelation in a falcon tube, then placed the tube at 37 °C before 3 mL of 37 °C NS was layered on top of the gel. At the specified timepoints (0 h, 2 h, 4 h, 6 h, 8 h, 24 h, 48 h, 72, and 120 h), 1 mL sample was taken out and filled up the volume with 1 mL fresh NS. FOLactis concentrations were detected by ELISA set on 600 nm. The cumulative release was calculated as follows:

$$E(\%) = (V_E \Sigma_1^{n-1} C_i + V_0 C_n)/m_0 \times 100$$

E(%) is the cumulative release, V_E is the withdrawn volume (1 mL), V_0 is the beginning volume (3 mL), C_i and C_n are the FOLactis concentrations, i and n are the sampling times, and m_0 is the total amount of FOLactis in the hydrogel (5×10^9 CFU).

In vitro FO fusion protein release: 10^{10} CFU FOLactis-sfGFP were dissolved in 500 μl PBS or 20 wt% P407 at 37 °C. At indicated time points, we obtained the supernatant by centrifugation (12,000×*g*, 4 °C and 5 min) and detected the fluorescence intensity of sfGFP using a Varioskan Lux microplate reader (Thermo Fisher Scientific). We extracted and purified FO-sfGFP from the lysates of 10^{10} CFU FOLactis-sfGFP as the total protein. The release rate of protein was calculated according to the following formula:

Release of protein (%) = Fluorescence intensity of FO – sfGFP / Fluorescence intensity of total FO - sfGFP

In vivo real-time near-infrared fluorescence imaging: NIR imaging was used to detect the extended storage and release of FOLactis in vivo when loading in P407 hydrogel. FOLactis were stained with DIR (Bridgen, Beijing, China) before subcutaneous injection in Balb/c mice. DIR was incubated with FOLactis at 37 °C for 20–30min, which was diluted to 5 μM as the previous work concentration previously. After centrifugation at 10,000*g* for 1min, resuspend the sediment in NS. This process was repeated 3 times. For quantitative localization of FOLactis, we injected DIR-stained FOLactis or FOLactis/P407 peritumorally after CT26 tumor cells inoculation for 1 week. Then, CRi Maestro In Vivo Imaging System (Cambridge Research & Instrumentation, Massachusetts, USA) was used to anesthetize and scan the mice at indicated time points since FOLactis or FOLactis/P407 administration. Tumors, TDLNs, and main organs, including heart, liver, spleen, lung, and kidney, were excised and imaged for removed tissue imaging after the mice were sacrificed under deep anesthesia.

Immunofluorescence confocal imaging: Immunofluorescence confocal imaging was employed to represent the trajectories of FOLactis in vivo. We harvested tumors, TDLNs, and main organs, including the heart, liver, spleen, lung, and kidney, after peritumoral injection of DiO-stained FOLactis at a certain time. After washing with PBS 3 times, the frozen sections were mounted with DAPI (Beyotime, Shanghai, China) and then imaged on a confocal laser scanning microscopy (Leica, Germany).

Immunohistochemistry analysis: Tumors were harvested 7 days after the last treatment and incubated paraformaldehyde-fixed tumor tissue sections with primary antibodies CD8 (EPR21769, Abcam) and CD11c (GB11059-100, Servicebio) overnight at 4 °C and then washed with PBS three times. The expression level of CD8 and CD11c were statistically analyzed and quantified by ImageJ v1.8.0.

Bacterial colonization in vivo: Bacterial colonization was used to calculate the distribution of bacteria ulteriorly. We harvested tumors, TDLNs, blood, and major organs at indicated times after peritumoral

injection of FOLactis or FOLactis/P407. The tissues were then weighed and grinded in NS at 4 °C. Homogenates were serially diluted to certain concentrations and plated on GM17 plates at 30 °C for 48 h. Bacterial colonies were counted and computed as CFU g^{-1} of tissue.

Tumor inoculation and therapy for subcutaneous models: 1×10^6 CT26 tumor cells in 100 μl NS were injected (*s.c.*) on the right lower sides of the abdomen for subcutaneous tumor effect experiments. The mice were randomly divided into 5 groups of different treatments ($n = 6$): [1] NS [2] P407 [3] Lactis [4] FOLactis [5] FOLactis/P407 when the tumor volume reached 100 mm^3 approximately. Tumors were treated via peritumoral injection with 10^{10} CFU Lactis, 10^{10} CFU FOLactis and 10^{10} CFU FOLactis/P407 on days 7, 14, and 21, which were dissolved in NS or 20% P407 to a final volume of 100 μl per dose. For the dose groping experiment, different concentrations of FOLactis or FOLactis/P407 were injected peritumorally as described above. Then the tumor volume, body weight and temperature of the mice were recorded every 2–3 days for 30 days. The tumor volume was counted via the following formula: $V = (\text{width})^2 \times \text{length}/2$. The upper tumor burden permitted was 1500 mm^3. At the end of treatment, the main organs, including the heart, liver, spleen, lung, and kidney were excised and then fixed in 4% paraformaldehyde, sectioned, and stained with H&E for safety analysis under optical microscopy (DM5000, Leica, Germany). Meanwhile, blood samples (~1.0 mL for each mouse) were also collected for blood biochemistry analysis to measure serum cytokines using LEGENDplex™ MU Th1/Th2 Panel (8-plex) w/VbP V03 (Biolegend).

Flow cytometry: All antibodies were maintained in the dark at 4 °C or −20 °C and prepared at the day of staining. Antibodies to CD11c (N418, FITC,117306), CD80 (1610A1,APC,104714), CD86 (GL1,PE,105008), CD103 (2E7,PerCP/Cyanine5.5,121448), CD3 (17A2,FITC,100204), CD8a (536.7,APC,100712), CD4 (GK1.5,PE/Cyanine7,100422), PD1 (29F.1A12,APC,123210), CD44 (IM7,PE,103008), CD49b (DX5, PE,108908), CD62L (MEL14,PE/Cyanine7,104418), CD11b (M1/70, FITC,101206), CD8a (536.7,PerCP/Cyanine5.5,100734), F4/80 (BM8, PE/Cyanine5,123112), CD206 (C06C2,APC,141708) were purchased from Biolegend.

The subcutaneous hydrogel was removed at the indicated time point after injection and placed at 4 °C for 1–2 h ， then we collected all cells in it for flow cytometry analysis through filtration. The mice that we harvested tumors, TDLNs (inguinal lymph nodes), and spleens used for flow cytometry were sacrificed 7 days post last treatment. The tumor tissues cut into pieces previously were digested with collagenase type IV (1 mg mL^{-1}, Sigma) for 2 h at 37 °C, and the single-cell suspension from the spleen and TDLN was prepared through mechanical lapping method. All samples were then resuspended in ice-cold NS, stained with specific antibodies for 20 min at 4 °C in darks, and washed 3 times before analysis. LEGENDplex™ MU Th1/Th2 Panel (8-plex) w/VbP V03 (Biolegend) was used to detect and analyze the level of cytokines in the tumor cell supernatant or serum. Cells were analyzed using Beckman CytoFLEX (Beckman, USA) and analyzed by FlowJo.

Tumor inoculation and therapy for intraperitoneal models: For CT26 mouse IP tumor models, 5×10^5 tumor cells suspended in 200 μl NS were intraperitoneally injected into the lower right abdomen of Balb/c mice. 7 days were allowed for tumor development before treatment, then the mice were randomly divided into 5 groups of different treatments ($n = 6$~7): [1] NS [2] P407 [3] Lactis [4] FOLactis [5] FOLactis/P407. Tumors were treated with intraperitoneal injection with 5×10^9 CFU Lactis, 5×10^9 CFU FOLactis and 5×10^9 CFU Lactis/P407 on days 7, 14, and 21, which were dissolved in NS or 15% P407 to a final volume of 200 μl per dose. We measured the body weight and temperature of the mice every 2–3 days for 30 days. Mice were euthanized at humane end points as soon as any following conditions were met: (i) moribund, (ii) weight loss or gain of >20%, or (iii) severe abdominal inflation. At the endpoint, we euthanized mice, then excised abdominal tumor nodules and IP fluid to assess tumor burden and immunotherapy efficacy induced by FOLactis/P407.

Tumor inoculation and therapy for orthotopic models: To develop orthotopic gastric cancer models, 5×10^5 MFC/MFC-Luc cells suspended in 50 μl NS were injected orthotopically into the stomach wall of 615 male mice [55]. The mice were randomly divided into 5 groups ($n = 4$) for different treatments 7 days after inoculation. 5×10^9 CFU Lactis, 5×10^9 CFU FOLactis and 5×10^9 CFU FOLactis/P407 which were dissolved in NS or 15% P407 to a final volume of 100 μl per dose were intraperitoneal injected to upper right abdomen of mice (near hepatogastric space) on days 7, 14, and 21. The body weight and temperature of the mice were recorded every 2–3 days for 27 days. We euthanized the mice and harvested stomach and abdominal disseminated nodules for assessment at the endpoint. In the MFC-GFP-Luc mouse tumor models, tumor burden was monitored on days 7, 17, and 27 after tumor inoculation through the IVIS Lumina III system (PerkinElmer, Massachusetts, USA). Before monitored, 200 μl D-luciferin at a concentration of 5 mg mL^{-1} was injected intraperitoneally into mice for fluorescence excitation.

Statistical Analysis: Statistical analysis was completed through GraphPad Prism 9.5.1. All results are presented as mean ± SEM for at least three independent experiments. For antitumor studies, there were 6–7 mice in each group. *p*-values were calculated by two-tailed unpaired Student's t-tests or two-way ANOVA and Tukey post-test and correction as indicated. Two-way analysis of variance (ANOVA) and one-way ANOVA with the Holm-Sidak multiple comparisons methods, were used to determine *p*-values for IVIS imaging datasets. $p < 0.05$ was considered as with statistical significance (ns $p > 0.05$, *$p < 0.05$, **$p < 0.01$, ***$p < 0.001$ and ****$p < 0.0001$). Figures were designed in Adobe Illustrator.

Ethics approval

All animal experiments were approved by the Laboratory Animal Care and Use Committee of the Affiliated Nanjing Drum Tower Hospital of Nanjing University Medical School (Checking number: 2022AE01021), and were carried out in compliance with all relevant ethical regulations.

Data availability statement

The data that support the findings of this study are available from the corresponding author upon reasonable request.

CRediT authorship contribution statement

Aoxing Chen: Writing – original draft, Visualization, Validation, Resources, Project administration, Methodology, Investigation, Formal analysis, Data curation, Conceptualization. **Junmeng Zhu:** Writing – review & editing, Software, Project administration, Investigation, Conceptualization. **Rui Liu:** Visualization, Supervision, Resources, Methodology, Investigation. **Yi Mei:** Software, Resources, Methodology, Formal analysis. **Lin Li:** Visualization, Software, Methodology. **Yue Fan:** Validation, Methodology, Investigation. **Yaohua Ke:** Writing – review & editing, Visualization, Methodology, Formal analysis. **Baorui Liu:** Writing – review & editing, Validation, Software, Project administration, Investigation, Funding acquisition, Formal analysis. **Qin Liu:** Writing – review & editing, Supervision, Software, Resources, Project administration, Investigation, Formal analysis, Conceptualization.

Conflict of Interest

The authors declare no conflict of interest.

Acknowledgements

A.C. and J.Z. contributed equally to this work. Thanks for Ying Chen (Nanjing University of Posts and Telecommunications)'s contribution to rheological measurements. This work was financially supported by the

National Natural Science Foundation of China (82272811 and 81930080) and the Fund for Distinguished Young Scholars of Jiangsu Province (BK20230001).

Appendix A. Supplementary data

Supplementary data to this article can be found online at https://doi.org/10.1016/j.bioactmat.2024.03.023.

References

[1] C.N. Baxevanis, S.A. Perez, M. Papamichail, Cancer immunotherapy, Crit. Rev. Clin. Lab Sci. 46 (4) (2009) 167–189.
[2] M. McNutt, Cancer immunotherapy, Science 342 (6165) (2013) 1417.
[3] I. Mellman, G. Coukos, G. Dranoff, Cancer immunotherapy comes of age, Nature 480 (7378) (2011) 480–489.
[4] Y. Zhang, Z. Zhang, The history and advances in cancer immunotherapy: understanding the characteristics of tumor-infiltrating immune cells and their therapeutic implications, Cell. Mol. Immunol. 17 (8) (2020) 807–821.
[5] Q. Li, Z. Shi, F. Zhang, W. Zeng, D. Zhu, L. Mei, Symphony of nanomaterials and immunotherapy based on the cancer-immunity cycle, Acta Pharm. Sin. B 12 (1) (2022) 107–134.
[6] M. Philip, A. Schietinger, CD8(+) T cell differentiation and dysfunction in cancer, Nat. Rev. Immunol. 22 (4) (2022) 209–223.
[7] W. Zou, Regulatory T cells, tumour immunity and immunotherapy, Nat. Rev. Immunol. 6 (4) (2006) 295–307.
[8] D.J. Propper, F.R. Balkwill, Harnessing cytokines and chemokines for cancer therapy, Nat. Rev. Clin. Oncol. 19 (4) (2022) 237–253.
[9] L. Hammerich, T.U. Marron, R. Upadhyay, J. Svensson-Arvelund, M. Dhainaut, S. Hussein, et al., Systemic clinical tumor regressions and potentiation of PD1 blockade with in situ vaccination, Nat. Med. 25 (5) (2019) 814–824.
[10] V. Durai, P. Bagadia, C.G. Briseno, D.J. Theisen, A. Iwata, JTt Davidson, et al., Altered compensatory cytokine signaling underlies the discrepancy between Flt3 (-/-) and Flt3l(-/-) mice, J. Exp. Med. 215 (5) (2018) 1417–1435.
[11] D. Endy, Foundations for engineering biology, Nature 438 (7067) (2005) 449–453.
[12] Y. Yu, T. Li, M. Ou, R. Luo, H. Chen, H. Ren, et al., OX40L-expressing M1-like macrophage exosomes for cancer immunotherapy, J. Contr. Release 365 (2024) 469–479.
[13] S. Kim, Y. Kim, S. Lee, Y. Kim, B. Jeon, H. Kim, et al., Live biotherapeutic Lactococcus lactis GEN3013 enhances antitumor efficacy of cancer treatment via modulation of cancer progression and immune system, Cancers 14 (17) (2022).
[14] L.F. Mager, R. Burkhard, N. Pett, N.C.A. Cooke, K. Brown, H. Ramay, et al., Microbiome-derived inosine modulates response to checkpoint inhibitor immunotherapy, Science 369 (6510) (2020) 1481–1489.
[15] J. Zhu, Y. Ke, Q. Liu, J. Yang, F. Liu, R. Xu, et al., Engineered Lactococcus lactis secreting Flt3L and OX40 ligand for in situ vaccination-based cancer immunotherapy, Nat. Commun. 13 (1) (2022) 7466.
[16] K. Garbacz, Anticancer activity of lactic acid bacteria, Semin. Cancer Biol. 86 (Pt 3) (2022) 356–366.
[17] C.J. Breitbach, B.D. Lichty, J.C. Bell, Oncolytic viruses: therapeutics with an identity crisis, EBioMedicine 9 (2016) 31–36.
[18] C. Wang, N.F. Steinmetz, A combination of Cowpea Mosaic virus and immune checkpoint therapy synergistically improves therapeutic efficacy in three tumor models, Adv. Funct. Mater. 30 (27) (2020).
[19] M.R. Charbonneau, V.M. Isabella, N. Li, C.B. Kurtz, Developing a new class of engineered live bacterial therapeutics to treat human diseases, Nat. Commun. 11 (1) (2020) 1738.
[20] F. Wu, J. Liu, Decorated bacteria and the application in drug delivery, Adv. Drug Deliv. Rev. 188 (2022) 114443.
[21] D. Zhang, Y. Chu, H. Qian, L. Qian, J. Shao, Q. Xu, et al., Antitumor activity of thermosensitive hydrogels packaging gambogic acid nanoparticles and tumor-penetrating peptide iRGD against gastric cancer, Int. J. Nanomed. 15 (2020) 735–747.
[22] Q. Liu, D. Zhang, H. Qian, Y. Chu, Y. Yang, J. Shao, et al., Superior antitumor efficacy of IFN-alpha2b-Incorporated photo-cross-linked hydrogels combined with T cell transfer and low-dose irradiation against gastric cancer, Int. J. Nanomed. 15 (2020) 3669–3680.
[23] Q. Hu, H. Li, E. Archibong, Q. Chen, H. Ruan, S. Ahn, et al., Inhibition of post-surgery tumour recurrence via a hydrogel releasing CAR-T cells and anti-PDL1-conjugated platelets, Nat. Biomed. Eng. 5 (9) (2021) 1038–1047.
[24] T. Chen, W. Zeng, C. Tie, M. Yu, H. Hao, Y. Deng, et al., Engineered gold/black phosphorus nanoplatforms with remodeling tumor microenvironment for sonoactivated catalytic tumor theranostics, Bioact. Mater. 10 (2022) 515–525.
[25] A.C. Daly, L. Riley, T. Segura, J.A. Burdick, Hydrogel microparticles for biomedical applications, Nat. Rev. Mater. 5 (1) (2020) 20–43.
[26] Z. Lv, T. Hu, Y. Bian, G. Wang, Z. Wu, H. Li, et al., A MgFe-LDH nanosheet-incorporated smart thermo-responsive hydrogel with controllable growth factor releasing capability for bone regeneration, Adv. Mater. 35 (5) (2023) e2206545.
[27] G. Dumortier, J.L. Grossiord, F. Agnely, J.C. Chaumeil, A review of poloxamer 407 pharmaceutical and pharmacological characteristics, Pharm Res. 23 (12) (2006) 2709–2728.
[28] M.S. Akash, K. Rehman, Recent progress in biomedical applications of Pluronic (PF127): pharmaceutical perspectives, J. Contr. Release 209 (2015) 120–138.
[29] J. Li, H. Ren, Q. Qiu, X. Yang, J. Zhang, C. Zhang, et al., Manganese coordination micelles that activate stimulator of interferon genes and capture in situ tumor antigens for cancer metalloimmunotherapy, ACS Nano 16 (10) (2022) 16909–16923.
[30] J. Kim, D.M. Francis, L.F. Sestito, P.A. Archer, M.P. Manspeaker, M.J. O'Melia, et al., Thermosensitive hydrogel releasing nitric oxide donor and anti-CTLA-4 micelles for anti-tumor immunotherapy, Nat. Commun. 13 (1) (2022) 1479.
[31] J.H. Choi, J.Y. Jang, Y.K. Joung, M.H. Kwon, K.D. Park, Intracellular delivery and anti-cancer effect of self-assembled heparin-Pluronic nanogels with RNase A, J. Contr. Release 147 (3) (2010) 420–427.
[32] E. Giuliano, D. Paolino, M. Fresta, D. Cosco, Mucosal applications of poloxamer 407-based hydrogels: an overview, Pharmaceutics 10 (3) (2018).
[33] V. Saxena, M.D. Hussain, Poloxamer 407/TPGS mixed micelles for delivery of gambogic acid to breast and multidrug-resistant cancer, Int. J. Nanomed. 7 (2012) 713–721.
[34] J.B. da Silva, M.T. Cook, M.L. Bruschi, Thermoresponsive systems composed of poloxamer 407 and HPMC or NaCMC: mechanical, rheological and sol-gel transition analysis, Carbohydr. Polym. 240 (2020) 116268.
[35] A. Frelet-Barrand, Lactococcus lactis, an attractive cell factory for the expression of functional membrane proteins, Biomolecules 12 (2) (2022).
[36] H. Cao, L. Duan, Y. Zhang, J. Cao, K. Zhang, Current hydrogel advances in physicochemical and biological response-driven biomedical application diversity, Signal Transduct. Targeted Ther. 6 (1) (2021) 426.
[37] Y.Z. Zhao, H.F. Lv, C.T. Lu, L.J. Chen, M. Lin, M. Zhang, et al., Evaluation of a novel thermosensitive heparin-poloxamer hydrogel for improving vascular anastomosis quality and safety in a rabbit model, PLoS One 8 (8) (2013) e73178.
[38] Y. Yu, R. Feng, J. Li, Y. Wang, Y. Song, G. Tan, et al., A hybrid genipin-crosslinked dual-sensitive hydrogel/nanostructured lipid carrier ocular drug delivery platform, Asian J. Pharm. Sci. 14 (4) (2019) 423–434.
[39] X. Yuan, X. Qin, D. Wang, Z. Zhang, X. Tang, X. Gao, et al., Mesenchymal stem cell therapy induces FLT3L and CD1c(+) dendritic cells in systemic lupus erythematosus patients, Nat. Commun. 10 (1) (2019) 2498.
[40] C.R. Gurbatri, I. Lia, R. Vincent, C. Coker, S. Castro, P.M. Treuting, et al., Engineered probiotics for local tumor delivery of checkpoint blockade nanobodies, Sci. Transl. Med. 12 (530) (2020).
[41] A.M. Duraj-Thatte, N.D. Courchesne, P. Praveschotinunt, J. Rutledge, Y. Lee, J. M. Karp, et al., Genetically programmable self-regenerating bacterial hydrogels, Adv. Mater. 31 (40) (2019) e1901826.
[42] H. Chen, Y. Guo, Z. Zhang, W. Mao, C. Shen, W. Xiong, et al., Symbiotic algae-bacteria dressing for producing hydrogen to accelerate diabetic wound healing, Nano Lett. 22 (1) (2022) 229–237.
[43] C. Liu, Y. Wang, P. Wang, Y. Gong, B. Yi, J. Ruan, et al., In situ electrospun aloe-nanofiber membrane for chronic wound healing, Smart Mater. Med. 4 (2023) 514–521.
[44] Z. Yang, Y. Zhu, Z. Dong, Y. Hao, C. Wang, Q. Li, et al., Engineering bioluminescent bacteria to boost photodynamic therapy and systemic anti-tumor immunity for synergistic cancer treatment, Biomaterials 281 (2022) 121332.
[45] D.W. Zheng, W.W. Deng, W.F. Song, C.C. Wu, J. Liu, S. Hong, et al., Biomaterial-mediated modulation of oral microbiota synergizes with PD-1 blockade in mice with oral squamous cell carcinoma, Nat. Biomed. Eng. 6 (1) (2022) 32–43.
[46] V. Moskovicz, R. Ben-El, G. Horev, B. Mizrahi, Skin microbiota dynamics following B. subtilis formulation challenge: an in vivo study in mice, BMC Microbiol. 21 (1) (2021) 231.
[47] J. Li, D.J. Mooney, Designing hydrogels for controlled drug delivery, Nat. Rev. Mater. 1 (12) (2016).
[48] H. du Bois, T.A. Heim, A.W. Lund, Tumor-draining lymph nodes: at the crossroads of metastasis and immunity, Sci. Immunol. 6 (63) (2021) eabg3551.
[49] D.M. Francis, M.P. Manspeaker, A. Schudel, L.F. Sestito, M.J. O'Melia, H.T. Kissick, et al., Blockade of immune checkpoints in lymph nodes through locoregional delivery augments cancer immunotherapy, Sci. Transl. Med. 12 (563) (2020).
[50] T. Aoyama, T. Yoshikawa, Adjuvant therapy for locally advanced gastric cancer, Surg. Today 47 (11) (2017) 1295–1302.
[51] W. Chen, K. Shi, J. Liu, P. Yang, R. Han, M. Pan, et al., Sustained co-delivery of 5-fluorouracil and cis-platinum via biodegradable thermo-sensitive hydrogel for intraoperative synergistic combination chemotherapy of gastric cancer, Bioact. Mater. 23 (2023) 1–15.
[52] R. Bhardwaj, J. Blanchard, Controlled-release delivery system for the alpha-MSH analog melanotan-I using poloxamer 407, J Pharm Sci 85 (9) (1996) 915–919.
[53] S.C. Chi, H.W. Jun, Release rates of ketoprofen from poloxamer gels in a membraneless diffusion cell, J Pharm Sci 80 (3) (1991) 280–283.
[54] C.K. Chung, M.F. Fransen, K. van der Maaden, Y. Campos, J. Garcia-Couce, D. Kralisch, et al., Thermosensitive hydrogels as sustained drug delivery system for CTLA-4 checkpoint blocking antibodies, J. Contr. Release 323 (2020) 1–11.
[55] T. Shi, Y. Zhang, Y. Wang, X. Song, H. Wang, X. Zhou, et al., DKK1 promotes tumor immune evasion and impedes anti-PD-1 treatment by inducing immunosuppressive macrophages in gastric cancer, Cancer Immunol. Res. 10 (12) (2022) 1506–1524.